

New Year 2022 Message

Technical Articles

- Organic Phase Mediated Dissolution of U-Zr Alloy: A Feasibility Study
- Nanometer-Scale Tribological Properties of Ultrananocrystalline Diamond Films

Young Officer's Forum

- Phase Transformation Studies Using Quench Deformation Dilatometer

News and Events

- 4th AC & Refrigeration Service Program - ACRESERVE 2021
- Dedication of 750 TR Capacity Centrifugal Chiller at Central Water Chilling Plant – II
- One Day Theme Meeting on SQUID Sensor and Its Applications
- 12th International Conference on Recent Advances in Information Technology (READIT)
- Participation and a medal by DAE in a Para-Badminton International 2021
- Technology Transfer of "Autonomous Gamma Dose Logger"

Awards, Honours and Recognitions

Back Cover: Indian Golden Oriole at Kalpakkam

From the Editor's Desk

Dear Reader

I wish you all a very Happy New Year.
May the New Year 2022 bring you more happiness, success, and good health.

It is my pleasant privilege to forward the latest issue of IGC Newsletter (Volume 131, January 2022, Issue 1). I thank my team for their timely inputs, cooperation and support in bringing out this issue.

The New year message of Dr. B. Venkatraman, Distinguished Scientist, Director, IGCAR, is included in this issue.

The digital copy is published through the websites <http://vaigai> and <http://www.igcar.gov.in>.

The first technical article is on "Organic phase mediated dissolution of U-Zr alloy: A feasibility study", contributed by Mr. Alok Rout and Colleagues from Materials Chemistry and Metal Fuel Cycle Group.

The second technical article is contributed by Mr. S. Sengottuvel and his colleagues from the Materials Science Group titled "Nanometer-Scale Tribological Properties of Ultrananocrystalline Diamond Films".

Young Officer's Forum features an article on "Phase Transformation Studies Using Quench Deformation Dilatometer", by Mr. S. Haribabu from Metallurgy & Materials Group, IGCAR.

We are happy to share with you the awards, honours and distinctions earned by our colleagues and about the important events.

In this issue An Indian Golden Oriole photographed in the DAE campus is on display.

The Editorial Committee would like to thank all the contributors. We look forward to receiving constructive suggestions from readers towards improving the IGC Newsletter content.

Use Face Mask. Maintain Social Distance to break the chain. Vaccinate. Stay Safe.

With best wishes and regards

S. Rajeswari
Chairman, Editorial Committee, IGC Newsletter and
Head, Scientific Information Resource Division, IGCAR

New Year 2022 Message

Dear Colleagues,

It is my pleasure to wish all our colleagues in Indira Gandhi Centre for Atomic Research (IGCAR), Bharatiya Nabhikiya Vidyut Nigam (BHAVINI), General Services Organization (GSO) and their families a very joyous, pleasant, healthy, blissful and prosperous New Year 2022.

This year again, the battle with COVID19 pandemic continued with much more vigour to quell the second wave in the middle months of the year. GSO and the Medical Group in particular, have put in painstaking efforts to tide over the crisis. Their efforts towards sanitization, isolation of patients, systematic triaging, organizing vaccination drives and other efforts towards containing the pandemic is highly commendable. These efforts have helped in almost near normal functioning of the various Units in DAE Complex at Kalpakkam.

It is heartening to note that in spite of the pandemic situation, we have been able to put in our best efforts towards keeping up the momentum for accomplishing our goals. It is the time of the year to take stock of the credits earned and to set our goals firmly for moving ahead for earning greater achievements in 2022.

The Fast Breeder Test Reactor (FBTR), the flagship reactor of the 2nd stage of the Indian Nuclear Power Programme has successfully completed 29 irradiation campaigns since its inception in 1985. Regulatory clearance has been obtained for commencing the 30th irradiation campaign, during which reactor power is planned to be raised to its rated power of 40 MWt for the first time. The U-233 fuelled Kalpakkam Mini Reactor (KAMINI) continued to be operated for neutron radiography of active & inactive components and activation analysis.

At COmpact Reprocessing facility for Advanced fuels in Lead shielded cells (CORAL), three campaigns have been completed successfully for reprocessing of the FBTR fuel. This is an important milestone in the performance record of this facility, which has operated well beyond its designed life time. Current emphasis is on the effective reduction in man-rem, even while meeting the stringent norms of fuel fabrication.

The Demonstration Fast Reactor Fuel Reprocessing plant (DFRP) is in the second stage of commissioning, viz. commencing of Acid-TBP runs, the commissioning of the Inter-cell Transfer Trolley



Systems, performance testing of diluents wash units, centrifuge, vacuum aided airlift transfers and erection of three remote sampling stations in the Sampling cell. Alternate U-Pu flowsheet has been developed for achieving higher decontamination factors in mass transfer equipment with multiple scrub acidities, which is vital towards reducing uranium load in reprocessing plants.

Injection casting system (IC) with a capacity of 10 kg has been augmented and optimized for all the process parameters towards casting U-6wt% Zr to be used as blanket slug as well as for the R&D studies towards aqueous and pyrochemical reprocessing studies. About 50 slugs of U-Zr of required dimensions have been successfully fabricated. Slugs prepared using the injection casting have been characterized for parameters such as density, dimensions, surface finish and also for metallic and non-metallic impurities. Fabrication of U-Zr slugs is in progress for delayed neutron detection (DND) application.

In our endeavour towards indigenous development of improved materials and processes, single crystals of Lead Zinc Niobate – Lead Titanate (PZN-PT) has been indigenously grown and characterized for development of surface acoustic wave devices. Thermo-vacuum process has been successfully deployed for the first time for regeneration of cold-trap of a mini-sodium loop in-situ. Hydrogen sensors both in-sodium and in argon gas phase, developed in-house, have been deployed to monitor the cold-trap regeneration process for the first time successfully. A new approach to enhance magnetic heating efficiency at acidic pH for magnetic nano-emulsions has been developed for the first

time. Medium (5-6 mm) and large thickness (10-11 mm) plates of 316 LN stainless steel has been successfully welded using autogenously activated TIG, Laser and Hybrid laser-MIG welding techniques.

Facilities such as RISHI (Research Facility for Irradiation Studies in Sodium at High Temperatures) loop (under the DAE-CEA collaboration of JHR (Jules Horowitz Reactor), has been conceptualized, designed and developed. A model gas extraction facility has been designed, fabricated in-house and successfully demonstrated for the quantitative recovery of krypton and xenon from sodium.

A Chemical Emergency Response System (CERS) has been developed based on the augmented Online Decision Support System (ONERS) of IGCAR, in collaboration with the Department of Factories and Boilers (FAB), Government of Kerala and NRSC-ISRO for assessing the impact of toxic gas releases at industrial sites. Also, a new approach to study the East Coast Cyclonic Storm Data for estimation of severe wind hazard for Kalpakkam Coast has been developed. IGCAR and ISRO would be jointly pursuing a green cover estimation of the DAE complex at Kalpakkam for sustainable environmental management of future projects. As a first step towards enhancing the vegetation density in Kalpakkam campus, about 5000 trees have been planted in the northern site. Field investigations and mapping of radioactivity levels in soils in different regions of Tamil Nadu has been initiated in collaboration with Government College, Tiruvannamalai and Scott Christian College, Nagercoil.

The technologies for the development of "Pulsating Sensor-based Conductivity Meter", "Portable High Volume Air Sampler" and "Autonomous Gamma Dose Logger" developed under "Atma Nirbhar Bharat" programmes of IGCAR have been successfully transferred to industry.

Thirty young trained scientists and engineers (OCES-2020, 15th Batch) have successfully completed their orientation programme at BARC Training School at IGCAR and were placed in various units of DAE. The programmes of HBNI continue to progress with full vigour. Also, around one hundred and thirty-five category I & II trainees have completed their classroom training and are presently pursuing their on-the-job training.

The Prototype Fast Breeder Reactor (PFBR) at BHAVINI is in an advanced stage of integrated commissioning with successive milestones like filling up of sodium in main vessel, commissioning of Safety Grade Decay Heat Removal (SGDHR) purification circuit-1, installation of inspection technologies for various components and inaccessible systems etc. progressing at

expected schedules. Fissile Zone Identification System deploying cadmium zinc telluride detectors and handing over of in-house manufactured four 170 m³/hour capacity Annual Linear Induction Pumps of modified design overcoming many challenges, resulting in substantial savings in both time and cost are some of the significant milestones that have been completed. A significant number of employees from various disciplines in IGCAR have been deployed to BHAVINI to coordinate and closely interact with the colleagues there, towards expediting the commissioning activities.

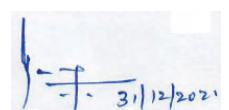
GSO continues to increase the numbers of dwelling units including refurbishment and enhancement of the infrastructural and medical facilities in both the townships. DAE Hospital continues to provide excellent health care to the residents of the townships. This year an outsourced (Apollo Hospitals) Dialysis Facility has been made operational at the DAE hospital, Kalpakkam which is a boon to dialysis patients who need not travel to Chennai and wait for appointments. The efforts put in by employees of GSO in maintaining the townships serene, green and clean is commendable. I sincerely thank the Principal, teachers and staff of all the Kendriya Vidyalayas and Atomic Energy Central Schools for their untiring efforts in organizing classes through virtual mode early this year and subsequently migrating to the offline mode in line with the COVID SOP, with the easing of restrictions. The performance of the students in board exams from all the five schools has been exemplary.

The Administration, Accounts and Auxiliary Departments of IGCAR and GSO have continued to provide commendable services guiding and supporting the execution of the programmes.

All these achievements would have been impossible, but for the tireless and sincere efforts put in by all of the employees. I take this opportunity to thank one and all.

The year ahead has a number of challenges in various domains. Foremost being achieving the milestone activities of PFBR viz. Main Vessel sodium filling and first approach to criticality, through joint efforts by BHAVINI and IGCAR, operation of FBTR to its rated capacity of 40 MWt and commissioning of DFRP.

I look forward to your continued support and co-operation towards the mandated activities and gaining more satisfaction levels in the official and personal fronts in the coming year.



(B. Venkatraman)

Organic Phase Mediated Dissolution of U-Zr Alloy: A Feasibility Study

Metal Fuels are the innovative choice for the fast breeder reactor due to their superior thermal and nuclear properties. Metal fuel has excellent steady state irradiation performance characteristics when adequate space is available to form interconnected porosity allowing fission gas release. As far as the Indian fast breeder reactor (FBR) is concerned, metallic fuel comprising of U-Zr and U-Pu-Zr alloy are considered as the candidate nuclear fuel. U-Zr and U-Pu-Zr alloys have high thermal conductivity, higher fissile atom density, higher breeding capacity, and lower doubling time over other types of ceramic fuels. About 6–10 % of zirconium has been added to these metallic actinides (U & Pu) to increase the melting temperature of the resultant U-Zr and U-Pu-Zr alloys. As an alternative to the pyrochemical process, the aqueous route (well-known PUREX (Plutonium Uranium Reduction EXtraction) process) is the best suited option for the reprocessing of the spent metal fuel. Reprocessing of the metallic spent fuel by the PUREX process (1.1 M TBP/ *n*-DD) requires the feed dissolver solution of the spent metallic fuel in nitric acid medium and to get the same, it is essential to dissolve the metalloids: U-Zr/U-Pu-Zr in nitric acid. Moreover, the separation of uranium from zirconium is required as the former is the fertile material for running a fast breeder reactor with plutonium as the driving fuel. Dissolution of U-Zr alloy in nitric acid medium requires a high concentration of nitric acid. To reduce the requirement of high concentration of nitric acid and have the feasibility of quantitative dissolution of U-Zr alloy, a novel technique was adopted in our laboratory involving an organic phase assisted dissolution process with a strongly hydrophobic and coordinating ligand named as N,N-dihexyloctanamide (DHOA). The ligand is a strongly coordinating CHON based extractant for hexavalent and tetravalent actinides. The structure of DHOA is given in Figure 1. Since it is a powerful lixiviant in its acid saturated condition, i.e., both leaching and

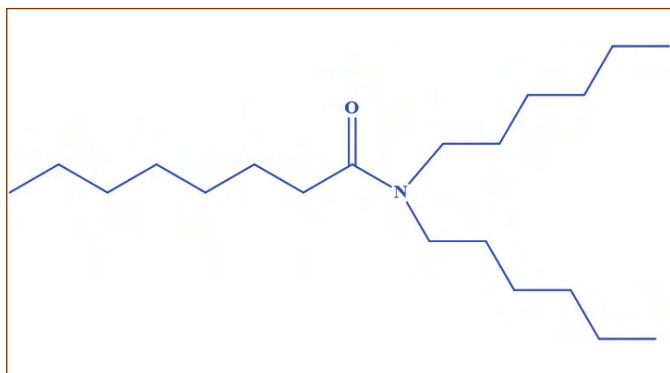


Figure 1: The structure of DHOA.

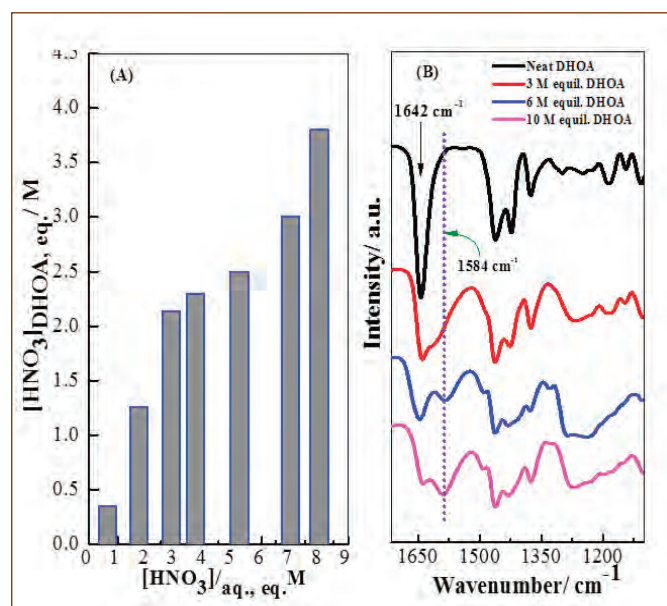


Figure 2: Nitric acid extraction by DHOA (A) and ATR-FTIR spectra (B) of DHOA before and after extraction. Aqueous phase = 1 M – 12 M HNO₃; T = 298 K; O/A = 1

extraction process occur in one step unlike nitric acid medium alone, it strongly binds with metal ion along with NO₃⁻ ion from the leached phase. Various experimental parameters for the dissolution process were tuned to ascertain the efficient dissolution of the alloy in DHOA phase and the detail results are narrated below.

Acid extraction by DHOA

Figure 2a shows the extraction of nitric acid by DHOA. The amount of nitric acid extracted by DHOA increases with an increase in the initial nitric acid concentration and ~ 4 M of nitric acid could be loaded in DHOA phase when the initial nitric acid concentration was 12 M. This is attributed to the presence of the carbonyl group (>C=O) in the molecule which gets protonated and hence enhances the formation of acid-solvate species.

Figure 2b exhibits the FTIR spectra of DHOA before and after acid equilibration. As expected, the band due to carbonyl moiety that gives the characteristic peak at 1642 cm⁻¹, gets broadened towards lower wave number upon acid extraction and a new peak at 1584 cm⁻¹ becomes more prominent with increase in the concentration of nitric acid indicating the protonation of DHOA.

Effect of initial acidity

Figure 3 displays the dissolution of U-Zr alloy as a function of

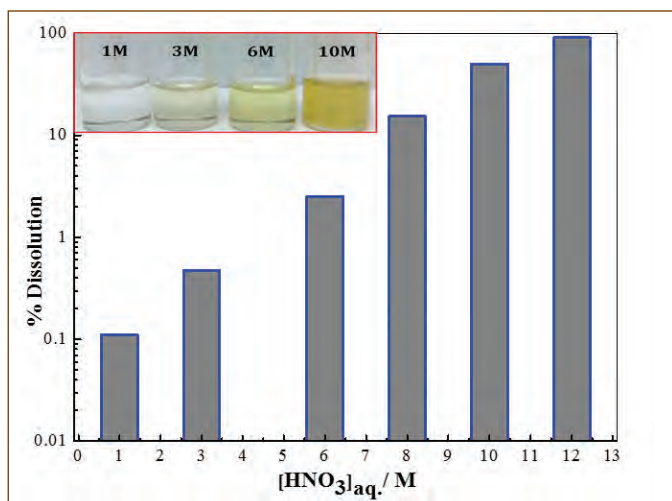


Figure 3: Dissolution of U – Zr alloy in DHOA phase as a function of aqueous phase nitric acid concentration. [HNO₃] = 1 M – 12 M; T = 353 K; Dissolution time = 6 hr; Initial weight of U – Zr alloy = 0.85 g; O/A = 1.

initial nitric acid concentration. The dissolution time was fixed at 6 hr and the experimental temperature was set at 353 K. It is noticed that the dissolution rate increases with an increase in the nitric acid concentration in DHOA phase and ~ 90% of the alloy was dissolved in 12 M nitric acid. It is anticipated that most of the dissolved metal ion would be uranium as the percentage of zirconium is only 6 % in it. The inset of Figure 3 indicates that the dissolution rate of uranium is more (as the color gets intense) at high nitric acid concentration.

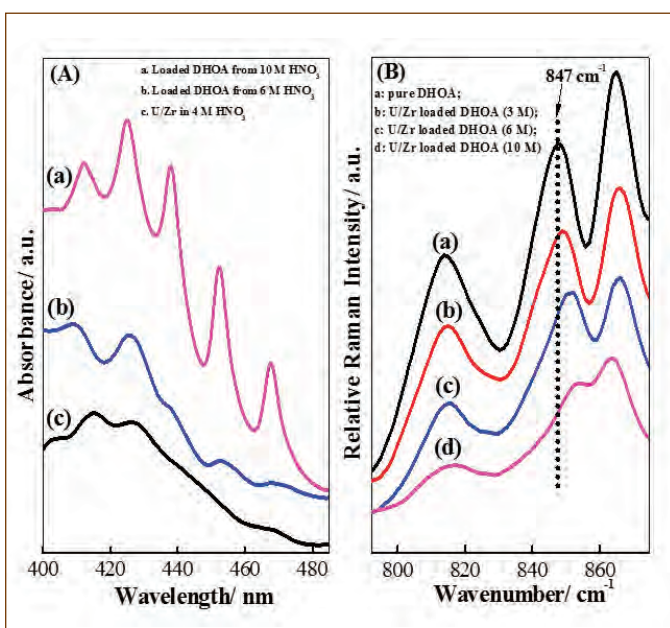


Figure 4: UV-Visible (A) and Raman (B) spectra of metal loaded DHOA phase. [HNO₃] = 6 M and 10 M (A) and 3 M – 10 M (B); T = 353 K; Dissolution time = 6 hr; Initial weight of U – Zr alloy = 0.85 g; O/A = 1.

In order to provide the supporting evidence for the metal loading in DHOA phase, Figure 4 displays the UV-Vis (4a) and Raman (4b) spectra of DHOA before and after metal loading. It can be seen from Figure 4a that the presence of uranium coordination in the organic phase shows different absorption patterns from that present in 4M nitric acid alone and with increasing nitric acid concentration, the simultaneous excitation of symmetric and unsymmetric bands of uranium loaded in DHOA phase is observed. However, the presence of very intense and sharp peaks is observed in case of 10 M nitric acid is attributed to the complex formation of the trinitrato complex of U(VI) ([UO₂(NO₃)₃]⁻) with the protonated DHOA ([HDHOA]⁺). It is the characteristic of DHOA that it exist as the protonated form upon equilibration with the nitric acid above 7 M.

Similarly, the Raman spectra confirm the presence of loaded metal ion in DHOA phase at a high nitric acid concentration by shifting the peak at 847 cm⁻¹ towards higher wave numbers. The peak at 847 cm⁻¹ is due to the bending vibration of NCO moiety present in DHOA. Besides, UO₂²⁺ has the symmetric U-O stretching vibration that occurs in the range of 800 cm⁻¹- 900 cm⁻¹ and the formation of UO₂(NO₃)₂ (or UO₂(NO₃)₂---DHOA) in the loaded organic phase occurs after 847 cm⁻¹. As a result, there is a shift in the peak position upon increasing the nitric acid concentration as the dissolution is more at high nitric acid concentration. These findings indicate the strong coordination of U(VI) with DHOA in the form of uranyl nitrate.

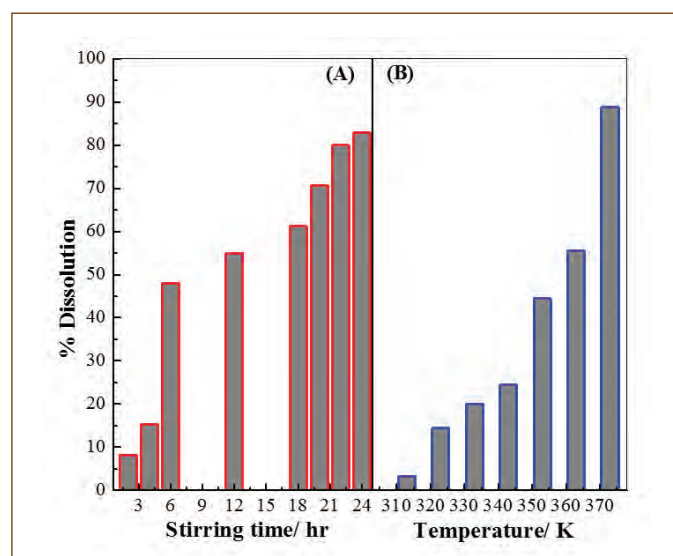


Figure 5 Dissolution of U – Zr alloy in DHOA phase as a function of dissolution time (A) and temperature (B). [HNO₃] = 10 M; T = 353 K; Dissolution time = 1 hr – 24 hr (A); Initial weight of U – Zr alloy = 0.85 g (A); O/A = 1 (A); Dissolution time = 6 hr (B); Initial weight of U – Zr alloy = 0.9 g (B); O/A = 1 (B).

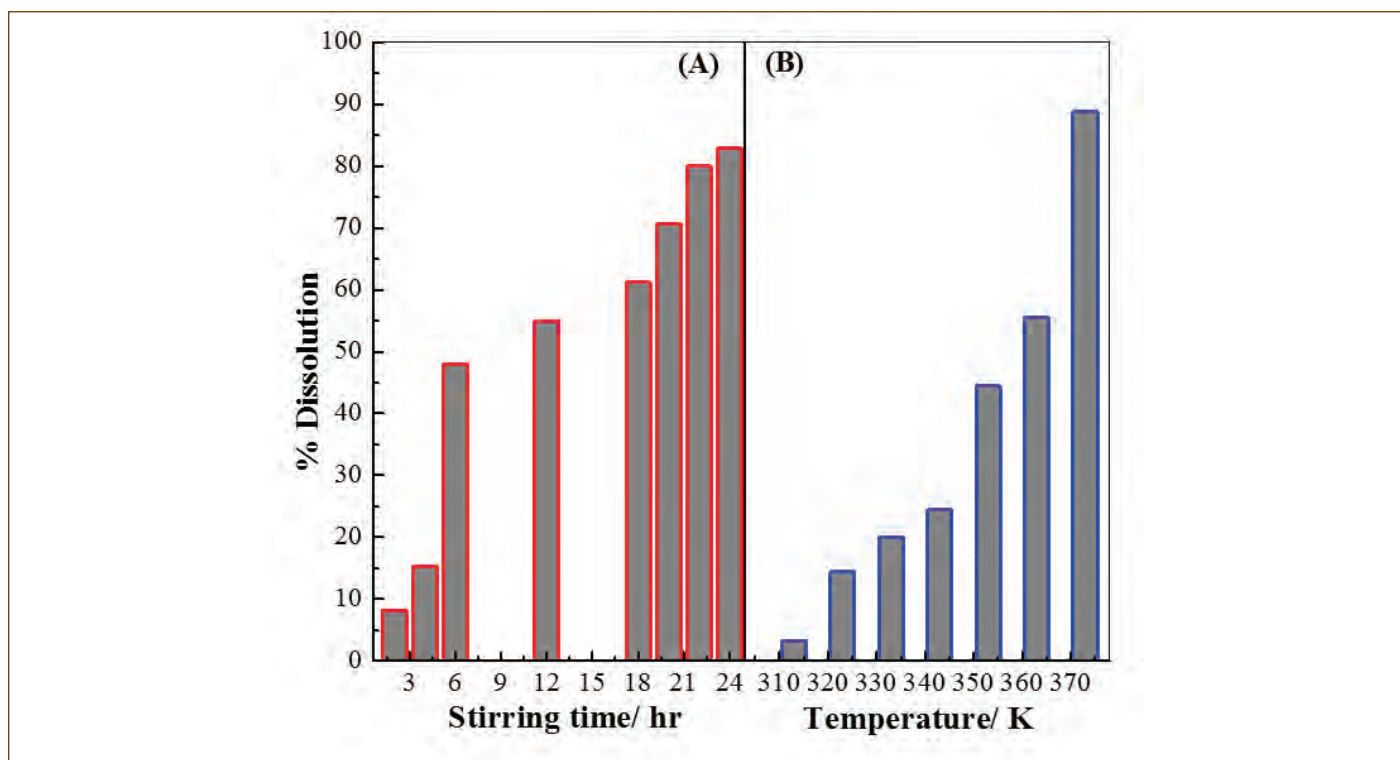


Figure 6: Dissolution of U – Zr alloy in DHOA phase as a function of volume of DHOA. $[\text{HNO}_3] = 10 \text{ M}$; $T = 353 \text{ K}$; Dissolution time = 6 hr (A); Initial weight of U – Zr alloy = 0.5 g; O/A = 1.

Effect of Dissolution time and Ligand volume

Dissolution time is an important parameter to acquire an adequate dissolution of the metal alloy. It was observed that an increase in dissolution time/stirring time enhances the dissolution process and $\sim 85\%$ U(VI) dissolution was achieved in 24 hr stirring at 353 K and 10 M nitric acid equilibrated DHOA phase (Figure 5a). Figure 5b refers to the effect of temperature on the dissolution speed. It was observed that the dissolution rate increases gradually with an increase in the experimental temperature and at 373 K, $\sim 88\%$ of U-Zr alloy was dissolved.

The plausible reason for the dissolution under these circumstances is attributed to the fact that the metallic bond between the metals in the alloy form gets weaker as the kinetic energy of the metal ion increases in the solvent phase upon increasing the temperature and stirring speed. It is essentially the reaction rate that effectively alters as a function of temperature – complexation between ligand and metal ion. The volume of the ligand was also varied to find out the extent of dissolution (Figure 6). It was observed that with an increase in acid loaded DHOA volume, the dissolution process becomes faster.

Stripping of dissolved metal ion from the loaded DHOA phase

The loaded organic phase, wherein, the maximum loading

was accomplished were taken and filtered leaving behind the segregated black residue sticking to the wall of the flask. In the subsequent step, the organic phase was dissolved in hexane for carrying out the stripping study. It is interesting to observe that it was possible to strip back all the metal ions within 3-4 contacts by using just Millipore water as the stripping solution. The recovered metal ions were then subjected to the ICP-AES analysis. As expected, the concentration of the recovered uranium was quantitative and that of zirconium was below the detection limit. Furthermore, during the stripping experiment using Millipore water, there was no precipitate observed neither in the stripped solution nor at the interface of the hexane and water phase affirming the absence of zirconium in the loaded organic phase. This therefore, confirms that quantitative amount of uranium from the alloy was dissolved and there was a negligible amount of zirconium dissolution. The present approach in other words, can also be explored to highlight the leaching of uranium from its alloy form with zirconium leading to high separation factor in the context of U/Zr separation.

Reported by
Alok Rout and Colleagues
Materials Chemistry and Metal Fuel Cycle Group

Nanometer-Scale Tribological Properties of Ultrananocrystalline Diamond Films

Friction and wear impose several challenges in mechanical assembly systems, and they lead to significant energy loss and frequent device failure. Over 20 % of energy consumed worldwide is lost due to friction or wear. Hence, the materials with ultralow friction and anti-wear characteristics are the most desirable in mechanical engineering applications where the carbon based materials have the potentials to play a major role. Since ultralow friction and negligible wear are demonstrated in ultrananocrystalline diamond (UNCD) and diamond-like carbon (DLC) films at ambient conditions, the research interest is ever increasing drastically over the recent past years. However, the origin of ultralow friction and high wear resistance in UNCD films is still under active debate because of the perplexed tribochemistry at the sliding interface.

There are numerous reports available in the literature on the factors affecting the ultralow friction and wear of UNCD and DLC films. The most acceptable postulates on ultralow friction and wear in UNCD and DLC are either due to surface passivation or rehybridization. Of them, the surface passivation is reasonably explained on the superlubricity in UNCD and DLC films based on tribotests at different environments. On the other hand, surface rehybridization, which occurs through the shear pressure leading to either amorphization or graphitization, is a complex phenomenon at atomic-scale with bond breaking and re-bonding at the sliding interface. The chemical and microstructure analysis of the tribofilm can provide invaluable information about the tribochemical reactions at the interface and the wear mechanism. The shear induced graphitization is mostly verified experimentally by observation of sp^2 and sp^1 rich a-C in the tribofilms which are studied by several analytical tools such as Raman spectroscopy, high resolution transmission electron microscopy (HRTEM), electron energy loss spectroscopy (EELS), X-ray photoelectron spectroscopy (XPS) and near-edge X-ray absorption fine structures. However, the obtained information is not limited to surface alone but includes a significant contribution from bulk and also, the spatial resolution is poor. Despite significant knowledge gained over the period, the microscopic mechanism of ultralow friction and wear in UNCD films are still not well understood.

Even though the concept of 2D graphene layer formation on tribofilms through shear induced graphitization is well recognized by both experimental and theoretical simulations, it is surprising to note here that direct micro-/nanoscopic evidences for the formation of layered graphene structures on tribotrack still lack in literature. This is mainly because of the challenges in distinguishing the atomically thin layers from rough wear track by the conventional microscopic techniques. Interestingly, an atomic

force microscope (AFM) can play a major role to study tribofilms since it can work from hundreds of micrometers down to atomic-scale. In addition, it also has several functional capabilities such as studying friction, elastic modulus, electrical and magnetic properties. Further, the frictional force microscope (FFM) has been explored in probing friction of carbon based materials and several other layered structures at nanometer-scale. Since the coefficient of friction (CoF) is different for various carboneous materials, a combined mapping of surface topography and friction would provide valuable information about the tribofilms.

In this study, two sets of UNCD films grown under Ar and N_2 atmospheres (labeled as UNCDAr and UNCDN, respectively) are considered for tribological analysis. In order to understand the origin of ultralow friction and wear, a systematic nanoscale friction analysis was performed using FFM inside the wear tracks that were run for different sliding distances, viz. 30, 100 and 500 m for UNCDAr and 2.5, 100, and 500 m for UNCDN films. Topography and friction force images are acquired simultaneously with soft Si cantilevers of $\sim 350 \mu\text{m}$ length and $\sim 0.05 \text{ N/m}$ spring constant. Further, FFM measurements are repeated on several locations in the wear track encompassing FLG nanostructures at different AFM tip scan velocities and normal loads.

Frictional force microscopy

Before going into the FFM analysis, a brief summary of macroscopic tribological properties are given here: The macroscale tribometric studies reveal that the UNCDAr films exhibit an ultrahigh wear resistance with an average saturated CoF of ~ 0.08 . Further, the CoF is high (~ 0.27) during the initial stage of sliding, and it gradually decreases to a lower value (0.08) after a long run-in distance of about 100 m. On the other hand, UNCDN films have ultralow friction with saturated CoF of ~ 0.04 with negligible run-in distance; however, the wear rate is relatively higher compared to UNCDAr films. The post wear analysis of the tribo tracks by Raman spectroscopy, HRTEM, EELS, and XPS analysis clearly revealed the presence of tribofilms with an excess amount of graphitic phase, but they could not provide a conclusive remark for the difference in the tribological properties of these UNCD films.

Figures 1a (1c) ((1e)) and 1b (1d) ((1f)) present the simultaneously acquired topography and friction force images, respectively, on wear track of UNCDAr film that undergone macroscopic wear test for a sliding distance of 30 m (100 m) ((500 m)). Note that the bright and dark areas in topography (FFM) represent the objects with maximum and minimum height (friction force), respectively. The wear track of UNCDAr film is partially worn out after 30 m

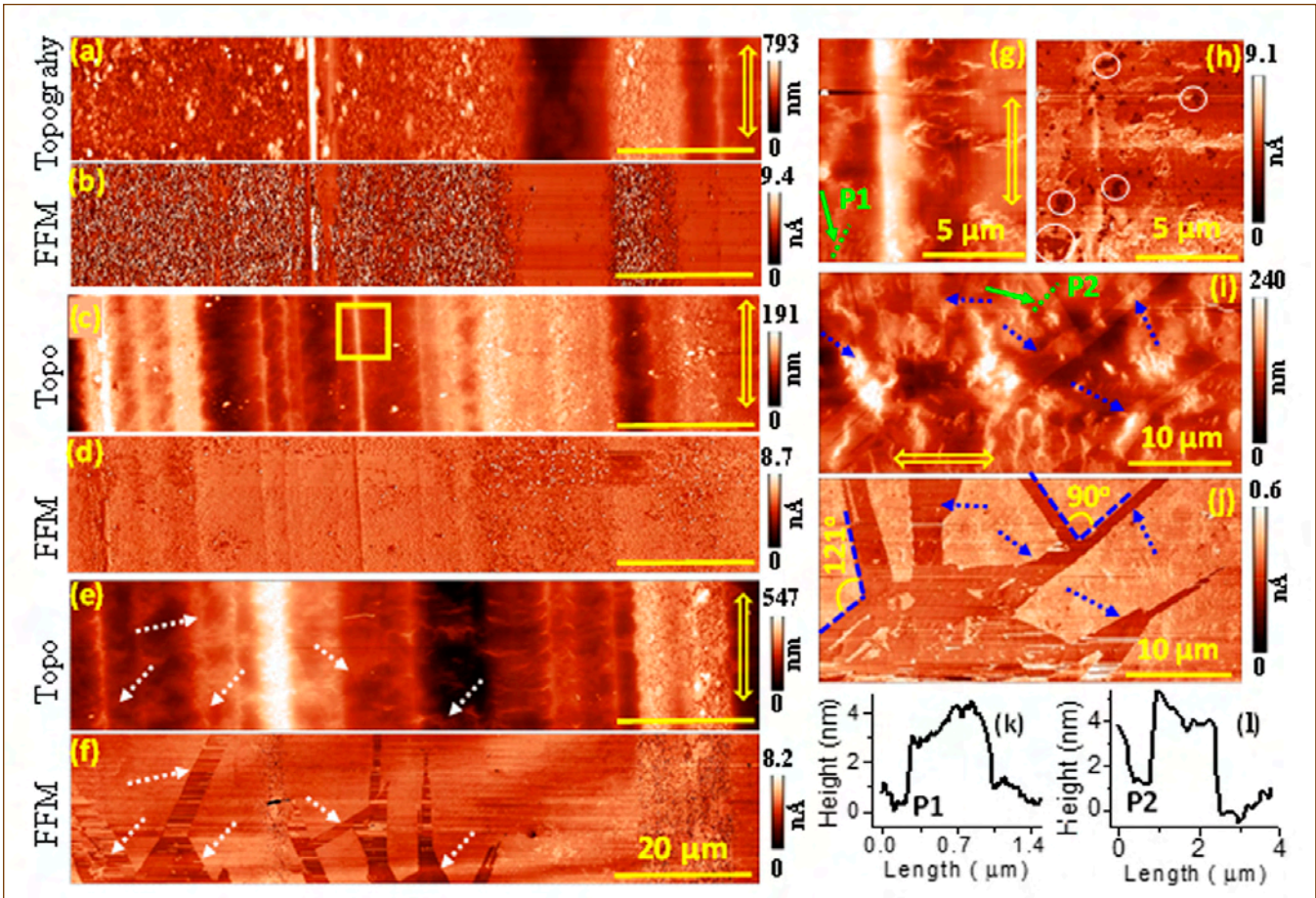


Figure 1: Simultaneously acquired AFM topography (a,c,e) and frictional force (b,d,f) images of the wear track in the UNCDAr that undergone wear test for the sliding distance of 30, 100 and 500 m, respectively. A magnified part of the topography (g) and friction (h) of wear track (100 m sliding distance, marked in image 1c). The selected area topography (i) and friction (j) of the wear track that ran for 500 m sliding distance. The height profiles across a FLG structures marked as P1 and P2 in Figure 1g and 1i are given in Figure 1k and 1l, respectively. The double arrow marks in the images (a, c, e, g, i) indicate the sliding direction. Scale bar = 20 μm for the images in 1a-1f.

run-in distance, as shown in Figure 1a, and the wear scratches introduce a very high root mean square (rms) roughness of 22.4 nm, measured over the entire image. The partially worn out surfaces have lower friction as compared to pristine surface, as can be seen in Figure 1b. After a sliding distance of 100 m, the surface of wear track is slightly smoothed due to the movement of tribofilms (rms roughness = 16.9 nm) as depicted in Figure 1c. The FFM image of the corresponding area in the wear track displays (Figure 1d) both low and high friction areas. A careful observation of the magnified part of the topography (Figure 1g) reveals the presence of secondary phase, over the tribofilm matrix, as isolated bright batches with a nearly flat top surface at an elevated height of (3.0 ± 1.0) nm and few hundreds of nanometer in lateral size in the wear track. The corresponding FFM mapping (Figure 1h) also displays dark regions (indicating lower friction force) wherever secondary phases are present in the tribofilms, and a few such areas are marked as circles in Figure 1h. The height profile of one such cluster labelled as P1 in Figure 1g is shown in Figure 1k, and it has a height of ~ 2 nm with a flat top surface and sharp edges at the periphery.

Figures 1e, 1i and 1f, 1j are topography and friction images, respectively, recorded at two different locations in wear track of UNCDAr films that ran for 500 m sliding distance. The calculated rms roughness is found to be 24.7 and 7.2 nm for the wear track shown in Figure 1e and 1i, respectively. Further, Figure 1i shows prominent and large networks of 2D nanoribbon like structures with a height of $\sim (3 \pm 2.0)$ nm and length $> 15 \mu\text{m}$. The width of the nanoribbons varies from ~ 1 to $10 \mu\text{m}$. A careful look at Figure 1e also reveals the presence of similar 2D nanoribbon networks and they are indicated by arrow marks as guide to eye. The presence of such 2D nanoribbons makes a striking difference in corresponding FFM images with the lowest friction values (dark regions), as illustrated by arrow marks in Figures. 1f and 1j. Figure 1l shows the height profile of one such nanoribbon indicated by an arrow in Figure 1i at position P2. The height and width of the nanoribbons are 4 nm and $1.8 \mu\text{m}$, respectively. In addition, these 2D nanoribbon structures are mostly oriented along the sliding direction, and a few branches are noticed in normal to the sliding direction. Apart from the large networks of

2D nanoribbon structures, there are also smaller clusters with unique friction characteristics in the wear track that was formed with 500 m sliding distance. On the other hand, such secondary phase nanoclusters or 2D nanoribbon structures with unique low friction characteristics are not detected on the wear track of UNCDAr films for the sliding distance of 30 m, even though UNCDAr films had undergone mild wear at this sliding distance. Note that the observation of 2D structures with atomic step height and flat top surface suggest the signature of FLG structures. Moreover, the observation of low friction on the FLG structures

reaffirms the presence of layered graphitic structure, which is well known for low friction. Here, the typical thickness of 2 nm indicates that the FLG structures have about five atomic layers of graphene since the monolayer graphene has a thickness of ~ 0.34 nm.

Figure 2a (2c) ((2e)) and 2b (2d) ((2f)) depict the topography and friction images respectively, in the wear track of UNCDN films that ran for 2.5 m (100 m) ((500 m)) sliding distances. The rms roughness of the wear track is about 27.9, 27.1 and 86.2 nm for the sliding distances of 2.5, 100 and 500 m, respectively. The

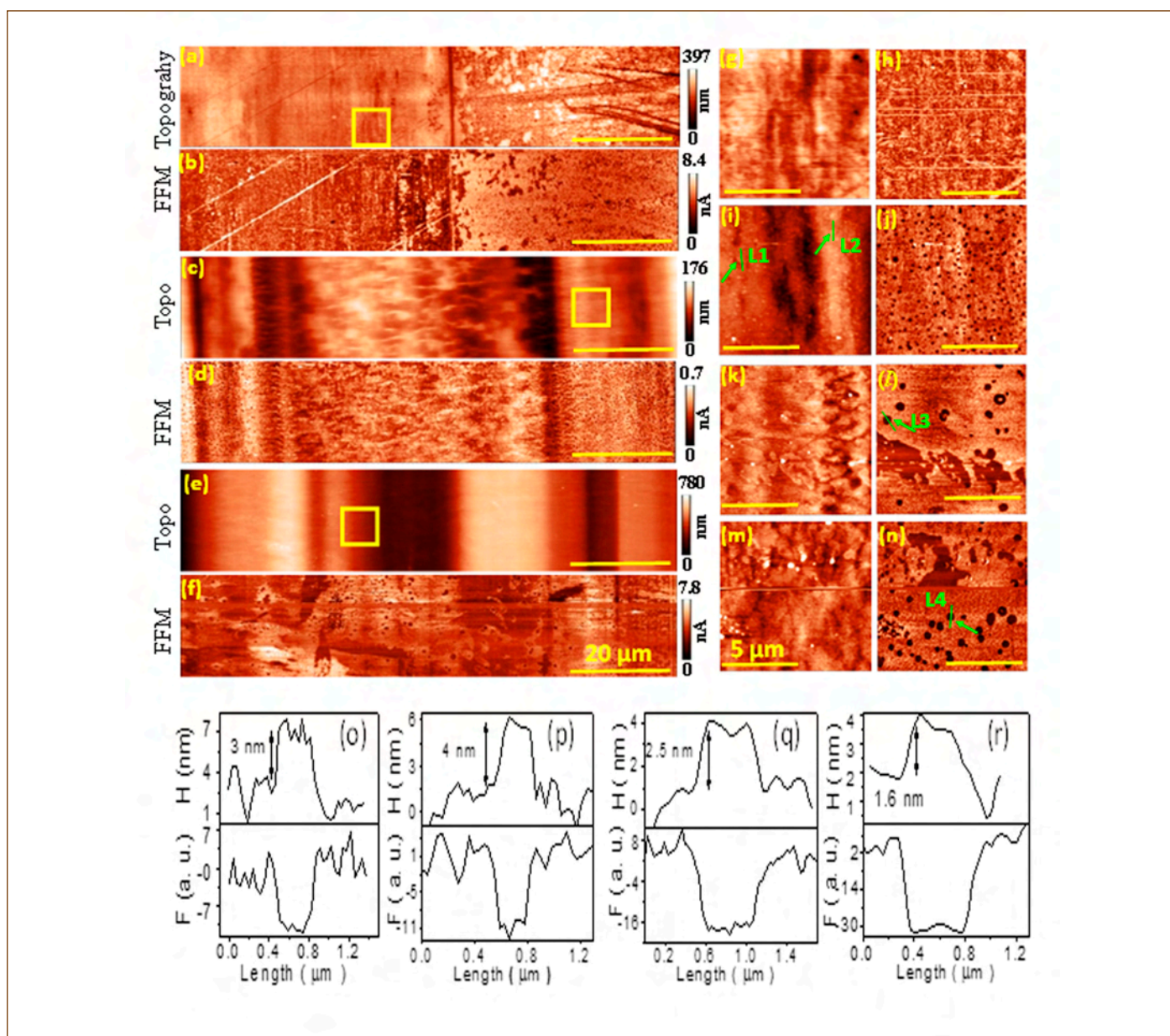


Figure 2: AFM topographies (a,c,e) and corresponding friction (b,d,f) images of UNCDN films measured inside the wear track that ran for 2.5, 100, and 500 m sliding distances, respectively. A magnified part of the topography and friction images (marked as square box area on the topographic images in Fig 2 (a,c,e)) are given in the images Figure 2(g,i,k) and Figure 2 (h,j,l), respectively. (m) Topography and (n) friction mapping recorded at different location in the wear track that undergone 500 m sliding distance. The scale bar is 20 and 5 μm for the images 2(a-f) and 2(g-l), respectively. The plots given in Fig 2o and 2p (2q and 2r) represent the line profile of height and corresponding friction force measured across graphitic structures on the wear track of 100 m (500 m) sliding distance, at the locations marked as L1, L2, L3 and L4.

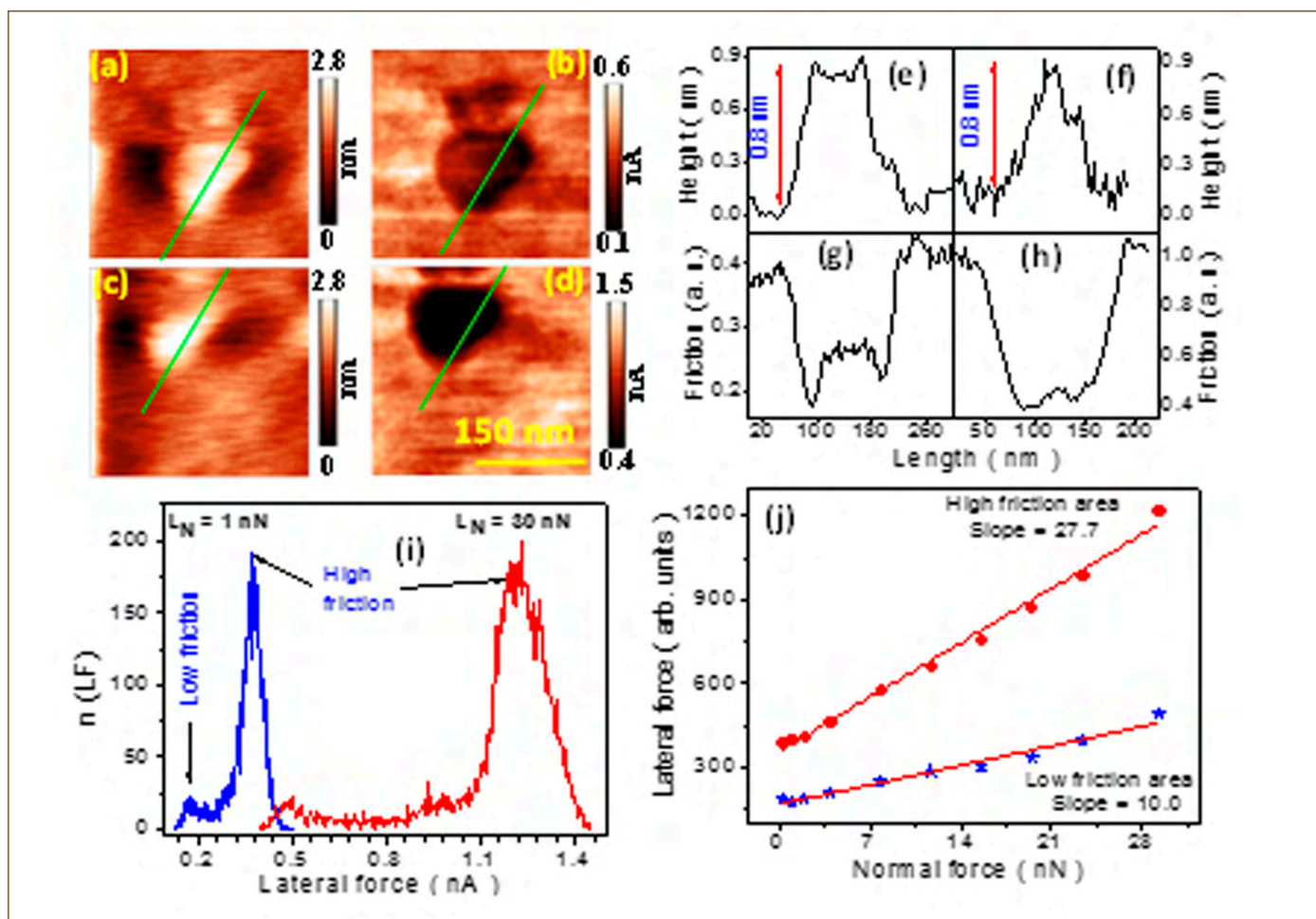


Figure 3: (a,c) Topography and (b,d) friction images on the wear track of UNCDAr measured at AFM tip normal load of (a,b) 1 and (c,d) 30 nN, respectively. (e-h) Line profiles of height and friction force measured on respective images of 3(a-d). (i) Histograms constructed from the friction force images given in Figure 3 b (the spectra in red color) and 3d (the spectra in blue color). (j) The variation of friction force as a function of normal load on UNCDAr film.

surface of the UNCDN films undergoes smoothing even after the sliding distance of 2.5 m (Figure 2a). With increasing the sliding distance to 100 m, the topography becomes much rougher due to the movement of tribofilms normal to the sliding direction (Figure 2c). After 500 m sliding, the wear track appears smooth due to the rearrangement of tribofilms. A magnified part of the topography and friction images of the wear tracks are shown in Figure 2g-2l. There is no signature of FLG secondary phases in the magnified part of the topography (Figure 2g) and friction mapping (Figure 2h) of wear track after 2.5 m sliding distance. After 100 m sliding distance, the friction mapping (Figure 2d and 2j) contains large number density of dark spots indicating lower friction areas in the wear track, which can be attributed to the presence of graphitic nanoclusters which are not obviously seen from topography (Figure 2c). However, the magnified part of the topography confirms the presence of FLG nanoclusters with a large number density in the wear track. Similarly, a large number of FLG nanoclusters are also present in the wear track that ran for a 500 m sliding distance (Figure 2k, 2m). Figures 2o and 2p (2q and 2r) show the line profile of height and friction

force recorded on selected FLG structures marked as L1 and L2 (L3 and L4) in Figure 2i and Figures 2l & 2n, respectively, on the wear track of 100 m (500 m) sliding distance. Moreover, based on height measurements, the average height and lateral size of the nanoclusters are $\sim (5.0 \pm 3.0) \text{ nm}$ [$(4 \pm 2.5) \text{ nm}$] and $(250 \pm 50) \text{ nm}$ [$(600 \pm 300) \text{ nm}$] for sliding distance of 100 m (500 m), respectively. These FLG nanostructures with uniform diameter are homogeneously distributed over the entire region of the wear track after sliding for 100 m, while the FLGs are inhomogeneously distributed over the entire region of the track after 500 m sliding distance.

For nanoscale friction analysis of these FLG nanostructures, FFM measurements were performed on a selected area by varying normal load. The sequence of friction images were recorded at constant normal load over a selected area, and for each image, the normal load on the AFM cantilever was increased in steps varying from 0.2 to 30 nN. Typical topography and friction images, recorded in the wear tracks of UNCDAr (500 m) for a normal load of 1 and 30 nN, respectively, are shown in Figures 3a, 3c

and 3b, 3d. The measured height of 0.8 nm indicates the presence of bilayer graphene in the selected region (Figure 3e, 3f). We also note here that the friction force signal was collected twice in each specified location, viz. during the forward and reverse scan of AFM tip and the net friction force mapping was constructed by subtracting one from the other. Subsequently, the distribution of friction force in a particular area is analyzed by constructing a histogram from each friction image and the typical histograms for the normal load of 1 and 30 nN are shown in Figure 3i. Further, the mean statistical friction force corresponding to the low (FLG structures) and high friction (matrix) regions are calculated from the histogram. These friction force values are plotted as a function of normal load, as shown in Figure 3j, and the slope of the plot gives the CoF. As shown in Figure 3j, the friction force increases as a function of normal load for both FLG nanoclusters and the a-C tribofilm matrix. The increase in friction is attributed to the puckering effect, which arises due to elastic deformation of the FLG structures with an increase in normal load. The weak Van der Waals force between the graphene layers allows puckering, which results in a reduction of the lateral dimension of the FLG structures, as can be seen from Figure 3d. Based on the slope of 10 and 27.7 (unnormalized), the relative CoF of FLG structure is about three times lower than the matrix in the track. A similar analysis is also performed for the wear track of UNCDN (500 m). In this wear track also the friction force increases with normal load. The slopes of the curves for FLG structures (low friction areas) and matrix (high friction areas) are found to be 3.1 and 5.4, respectively. As similar to UNCDAr films, the relative CoF is lower for FLG structures in UNCDN as compared to the matrix. In addition, the relative CoF of FLG structures and the matrix in UNCDN films is \sim three and five times lower than those of UNCDAr films, respectively. These results are consistent with

macroscopic tribo measurements, which shows the average saturated CoF of \sim 0.08 and 0.04 for UNCDAr and UNCDN films.

Further, the layered nature of the newly formed FLG structures and their binding on the tribofilms in the wear track are tested by measuring topography and friction mapping at a slightly higher normal load on the cantilever. Figures 4a and 4d show the simultaneously measured topography and friction force mapping on wear track of UNCDAr (500 m) at a normal load of 4 nN on the cantilever. As discussed earlier, the FLG structures have lower friction (darker area) as compared to the tribofilm of the matrix. Also, some part of the FLG structures (arrow mark in Figure 4a) has already started peeling off, and it is also reflected as bright areas in the FFM mapping (arrow mark in Figure 4d). Subsequent imaging at a higher load of 10 nN on the same location reveals that the FLG structures are completely removed from the matrix as can be seen from Figure 4b. It is also noticed that the previously known low friction area (darker regions) switches into higher friction area (bright regions in Figure 4e) immediately after the removal of FLGs. Moreover, the bright areas (high friction regions) on the right side ligament of the Y junction (Figure 4d) indicate that the partial FLG structures are peeled off during the forward scan, which is not reflected in the topography (Figure 4a). In order to verify the flipping of friction from low to high upon removal of FLG structures, an additional FFM measurement at 2 nN normal load was performed on a larger area encompassing the previously measured area, and the topography and FFM image are shown in Figure 4c and 4f, respectively. This measurement confirms the lower friction of FLG when the physical structure is intact (upper part of Figure 4c). Subsequently, after the FLG structures are physically removed, the underneath area becomes even higher in friction than

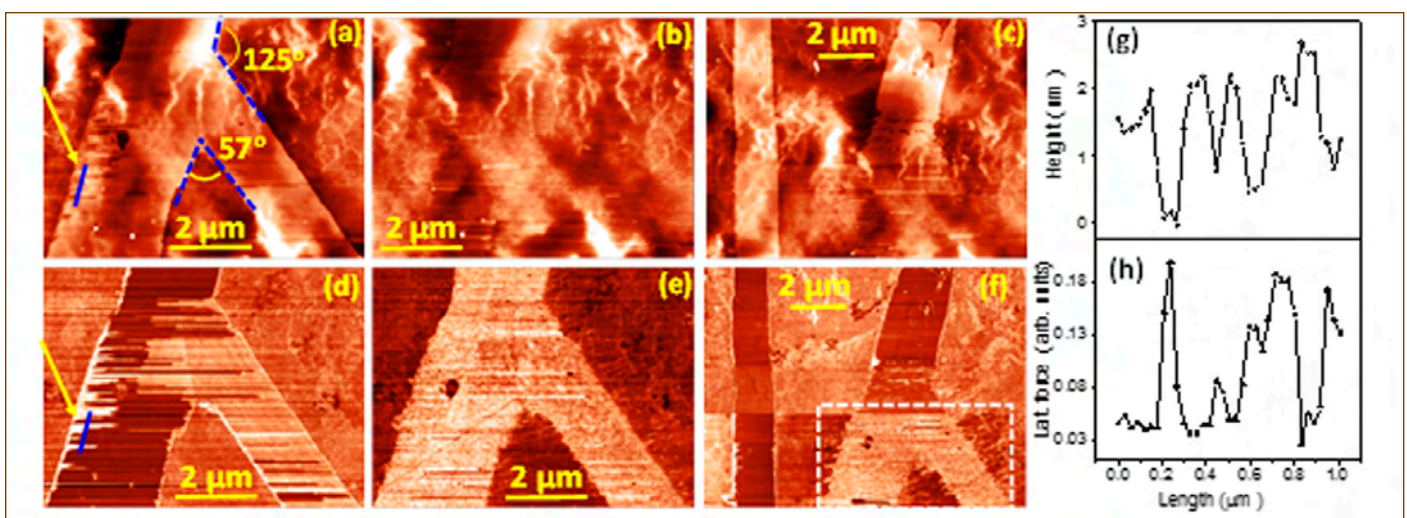


Figure 4: Simultaneously acquired topography and friction mapping on a few layer graphene structures. Mappings are recorded at normal load of 2 nN for the images given in 5a,5c,5d, and 5f, and at 10 nN for the images in 5b and 5e. The rectangle symbol on Figure 5f indicates the previously AFM measured area at higher load of 10 nN. The line profile of (g) height and (h) lateral force measured along the line marked in the image 5(a) and 5(d), respectively

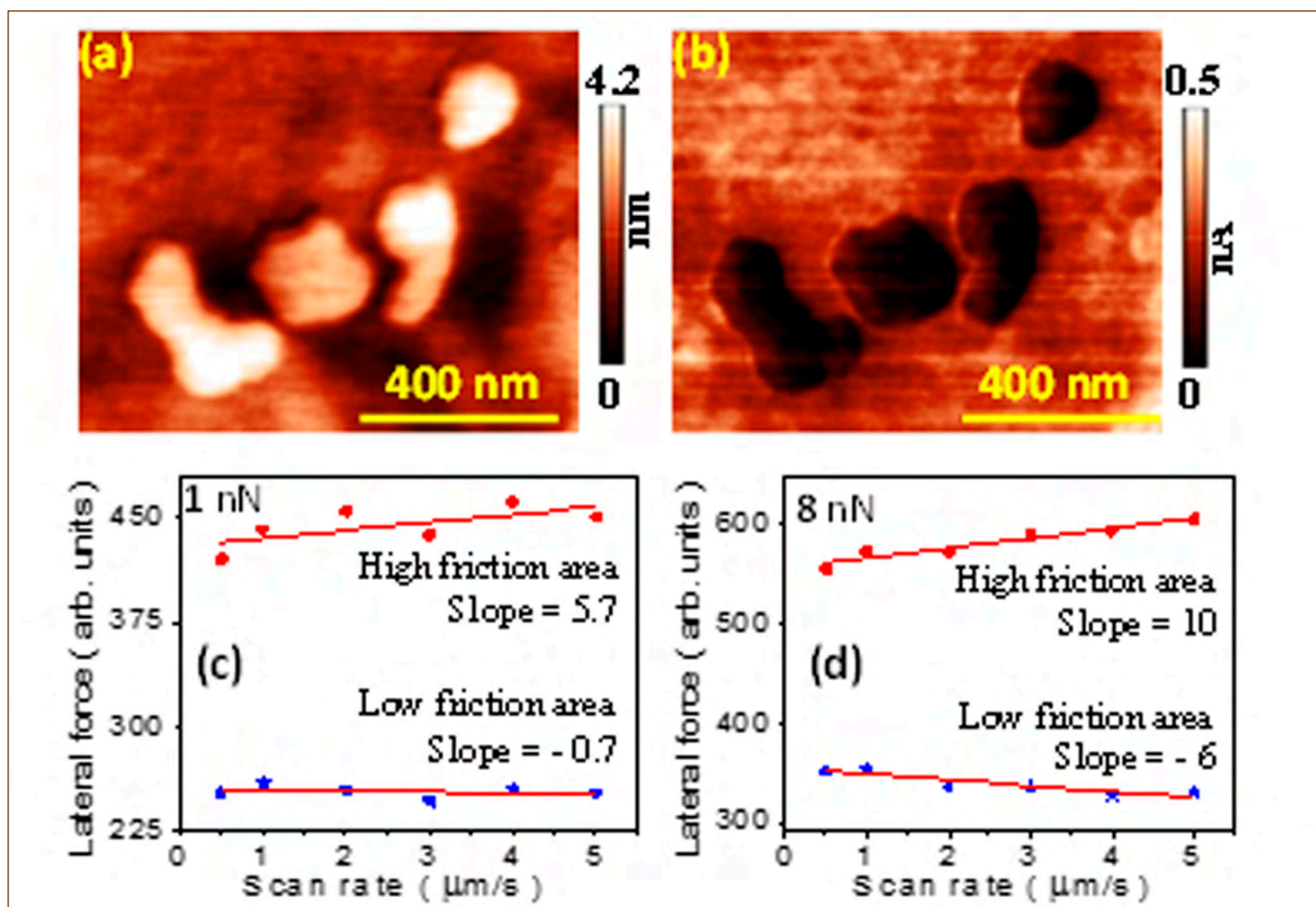


Figure 5: Simultaneously acquired topography (a) and friction (b) mapping on a few layer graphene structures, measured at normal load of 1 nN. The height of the individual structure is $\sim 1.6, 0.8, 2.4$ and 2.0 nm respectively, from left to right. The variation of lateral force as a function of AFM tip scan velocity at (c) 1 nN and (d) 8 nN normal loads indicating the opposite behavior of lateral force on low and high friction areas in the wear track.

the matrix. Since the friction measurements were performed immediately after removal of FLGs, the newly exposed area exhibits high friction due to the inherent nature of the tribofilms, which consist of highly disordered a-C with a large number of dangling bonds that increase the friction. In contrast, the smaller dimension FLG structures that are present on the wear track are not being completely removed, as compared to large networks of FLG. However, at a higher normal load on AFM tip, the smaller FLG structures undergo mechanical deformation as can be seen in Figure 3c.

In addition, the nanoscale frictional properties of the newly formed 2D structures are measured on the wear track of UNCDAr film by varying the tip scan velocity under constant normal loads of 1 and 8 nN. Figures 5a and 5b depict the topography and friction mapping, respectively, measured in the wear track at normal load of 1 nN. Here, the friction is lower on the 2D structures as compared to the matrix a-C tribolayer. Further, the sequence of friction images was recorded at constant normal load over a selected area, and for each image, the AFM tip scan velocity is varied from 0.5 to 5 $\mu\text{m/s}$. Then, a histogram is constructed for

each friction image to extract the average lateral force on the low and friction areas for different scan velocities. Figures 5c and 5d show the variation of lateral force as a function of scan velocity at a normal load of 1 and 8 nN, respectively. As can be seen from Figures 5c and 5d, the low and high friction areas display negative and positive slope for friction as a function of scan velocity. The negative slope of friction in the FLG nanocluster is attributed to meniscus force which arises due to the condensation of water molecules between tip and sample surface. The slower scan rate increases the contact area leading to higher friction, and also, this behavior indicates the hydrophilic nature of the FLG nanoclusters. On the other hand, the positive friction is associated with the hydrophobic character of a-C matrix. Though the friction measurements could not be performed under higher scan velocity due to structural deformation of FLG, this observation clearly reveals the different surface chemistry of FLG structures and a-C matrix.

Discussion

Based on the above results, it is proposed here that large

networks of FLG structures act as lubricant as well as protecting layers that results in ultralow friction and high wear resistance in UNCDAr films. On the other hand, the UNCDN films have a large number density of FLG nanoclusters which act as efficient lubricant resulting in ultralow friction. However, the high wear rate in UNCDN films can be associated with an inability to form larger networks of FLG nanostructures. Also, the adhesion of newly formed layered FLG structures over the a-C matrix tribofilm is poor. This results in removal of tribofilms in the wear track leading to a significant wear rate on both films. However, the higher wear rate in UNCDN films than that of the UNCDAr films can be associated with the tribofilms with higher sp² content, which are easily moved out of the track due to the roughness of the counter body.

Despite the above discussion, still the question remains that whether the newly formed low friction structures are few layer graphene or not. Or, is it sp²-rich a-C adlayer since there is no alternative direct evidence. Here, it is reiterated that the following evidences revealed by combined AFM and FFM measurements.

1. Atomic step height and low friction behavior of FLG structures as shown in Figures 1- 5.
2. Partial cleavage with sharp edges and variation of friction with the layer thickness (Figure 4)
3. Angles between adjacent edges are about 60, 90 and 120° as indicated in Figures 1 and 4. These angles are characteristic of graphene edge chirality that arises due to armchair and zigzag edges.
4. Friction force decreases with an increase in AFM tip scan velocity on FLG structures while an opposite behavior is observed for a-C matrix (Figure 5)

All the above mentioned four points are characteristics of layered graphene structures. Suppose if one is to assume the newly formed structure as sp²-rich a-C, it is impossible to cleave the partial top layer with sharp edges and also, the friction does not change with thickness. Moreover, the adhesion / surface chemistry cannot be opposite to the a-C matrix. Based on these facts, it is inferred that the newly formed tribolayers are indeed layered graphene structures. However, a direct measurement like tip enhanced Raman spectroscopy (TERS) can confirm the layered structure with distinct Raman characteristics of FLG structures. Also, HRTEM, scanning tunneling microscopy and Kelvin probe microscopy can shed more light on the layered nature of the FLG. Nevertheless, these techniques do also have several drawbacks to study of lateral tribolayers which are sparsely and randomly present on a rough wear track. Yet, AFM is a powerful and relatively simple tool, which helps to understand the complex wear track with the support of well-established characteristics of carbon materials.

Finally, it is very intuitive to know the driving force for the nucleation of ordered graphene structures over the tribolayers. Here, the rms roughness and wear test environments are almost identical for both the films, though the structural characteristics, sp³/sp² ratio, and hardness are different, and they might play a significant role on wear and friction. It is mostly accepted that the shear force induces sp³-sp² order – disorder transformation, which leads to the formation of sp²-rich a-C tribolayers at the sliding interface. Further, the shear localization mechanism suggests that rehybridization occurs at the tribo-interface with structural phase transformation, covalent bond reorientation and local structural ordering. Thus, the clusters of ordered crystallites with ~ 1 nm in size nucleate in the a-C matrix which has already been experimentally evidenced by HRTEM. However, it was not clear so far that whether these small crystallites grow into large size graphene layers or not. In fact, this work by AFM studies provide evidences of the growth of micro-/nanoclusters with ordered graphene layers or a large network of graphene nanoribbons in the wear track. Moreover, it should be noted here that the shear force induced energy dissipation at the sliding interface is very high for UNCDAr films due to the initial high CoF along with long run-in distance, high hardness and elastic modulus which are leading to the formation of large networked FLG structures. However, the energy dissipation is much lower for UNCDN films due to the higher sp² content, which makes negligible run-in distance and lower mechanical properties. Thus, the structural and mechanical properties play a significant role on the tribological properties of UNCD films.

In summary, the formation of the bilayer, trilayer, and a few layer graphene-like structures which arise due to shear induced graphitization are observed over the a-C tribofilms on two different sets of UNCD films using frictional force microscopy. Since the newly evolved few layer graphene structures act as lubricant as well as wear protector, UNCD films with large networked few layer graphene structures exhibit high wear resistance with low friction. In contrast, UNCD films only with isolated FLG structures display ultralow friction but it could not protect wear. In nutshell, the shear induced graphitization and the subsequent formation of ordered graphene layers play a major role on the ultralow friction and wear in UNCD films. Moreover, despite the 2D materials having an excellent frictional properties, they are easily affected by surface conditions, resulting in poor tribological results. Intensive study of atomic level friction using emerging 2D materials is need of the hour in the field of tribological research. Overall, the frictional force microscopy, combined with other macro-scale measurements, can serve as an excellent tool for understanding the tribology of carbon materials.

Reported by
S. Sengottuvel and his Colleagues
Materials Science Group

Young Officer's FORUM



Mr. S. Haribabu is Scientific officer 'D' in Physical Metallurgy Division, IGCAR. He is Gold medalist in B.Tech., Metallurgical & Materials Engg., Rajiv Gandhi University of knowledge technologies, AP. He is Homi Bhabha Gold Medalist from 59th batch of BARC training school. After joining IGCAR in 2016 he obtained M.Tech. from HBNI. His research areas include Phase transformation studies using dilatometry, Microstructural studies on additive manufactured materials & Materials modeling using ThermoCalc®/Dictra®.

Phase Transformation Studies Using Quench Deformation Dilatometer

Dilatometry is a powerful technique to study solid state phase transformations in materials. During phase transformation, there is underlying lattice structure change which is accompanied by a change in specific volume. According to Ehrenfest classification - jump in volume occurs for first order phase transformation and continuous volume change but discontinuity in the coefficient of Thermal Expansion (CTE) occurs for second order phase transformation. In the dilatometer, the change in specific volume is observed as a change in length. For example α -ferrite to γ -austenite transformation, while heating, in Fe based alloys results in reduction in volume which is seen as negative variation in length. If no phase transformation occurs - the thermal strain can be used to measure

coefficient of thermal expansion in materials. It is also possible to monitor real time dimensional variations in the specimen during thermal cycling.

State-of-the-art Quench Deformation Dilatometer (QDDL) with wide range of capabilities to study material phase transformation has recently been installed in PMD/MMG and is shown in Figure 1. It is equipped with water cooled Cu-induction coils allowing for instantaneous power transfer to the specimen with less thermal inertia. The dimensional variation in the specimen is transmitted through Quartz/Alumina push rod and measured using Linear Variable Differential Transformer (LVDT) in the longitudinal direction. Experiments can be performed under rapid heating and cooling rates applying tensile or compressive deformation either under vacuum or in He/Ar atmosphere. With the availability of LVDTs with an excellent resolution of 10 nm, it is now possible to study tempering stages and Time-Temperature-Precipitation diagrams as well. Various applications of QDDL includes study of phase transformation kinetics, measurement of CTE, generation of Continuous Heating Transformation (CHT), Continuous Cooling Transformation (CCT), Time Temperature Transformation (TTT), Time Temperature Transformation after Deformation (DTTT) and Time Temperature Precipitation (TTP) Diagrams, welding HAZ Simulations etc.

Three different operating modes available in QDDL are 1) Quenching mode 2) Compression mode and 3) Tensile mode. Schematic of the



Figure 1: Quench Deformation Dilatometer with subunits installed in PMD/MMG

Table 1 : Experimental parameters used in quenching and deformation modes in QDDL

Quenching Mode		Deformation Mode	
Temperature range	RT to 1600 °C	Temperature range	RT to 1600 °C
Sample geometry	Solid & Hollow	Deformation force	25 kN
Sample dimension	10x5 mm (LxDia.)	Deformation rate	0.01 to 200 mm/s
Heating rate	0.1 to 4000 °C/s	Heating rate	0.1 to 100 °C/s
Cooling rate	0.1 to 1600 °C/s	Cooling rate	100 °C/s
		Strain rate	0.001 to 20 /s
		True strain	0.05 to 1.2
		Deformation way	≥ 3 mm

arrangement to be adopted for each of these modes is shown in Figure 2 and further details are given below:

1) Quenching mode: In this mode (Figure 2(a)) the sample is in the form of a cylinder with 10mm length and 3-5mm diameter. Specimen can be heated up to 1600°C with heating rate varying from 0.1 to 4000°C/s. Temperature is measured using Type K or S thermocouple spot welded to the sample. Cooling is enabled through He/Ar gas flow control using servo valves. Cooling below room temperature is possible using liquid N₂. Experiments can be performed on non-conducting specimen also using a susceptor. An

optical displacement sensor attached to QDDL helps in detecting changes in the diameter of the specimen with a resolution of 150nm enabling estimation of total volume change in the sample.

2) Compression mode: In this mode (Figure 2(b)) specimen of 10mm length and 5mm diameter is supported by deformation punches made up of silicon nitride. Left and right punches have diameter and length of (15.5mm, 53mm) and (12.5mm, 38mm) respectively. To apply the force up to 25 kN and achieve a deformation rate of 0.01 to 200mm/s, the hydraulic punch on left side is driven using a servomotor. Heating and cooling rates of 0.1-100°C/s are achievable.

3) Tensile mode: Figure 2(c) shows that the specimen geometry to be used in tensile mode is quite different. Exact geometry and dimension of the specimen is given in Figure 3. Maximum thickness of the specimen is 1.5mm. Sample is screwed to stainless steel clamps on both sides and tensile deformation is applied from left side using hydraulic press. Details of various experimental parameters used in the quenching and deformation modes are listed in Table 1.

A brief description of the phase transformation studies carried out on reactor structural materials using QDDL is given in the following

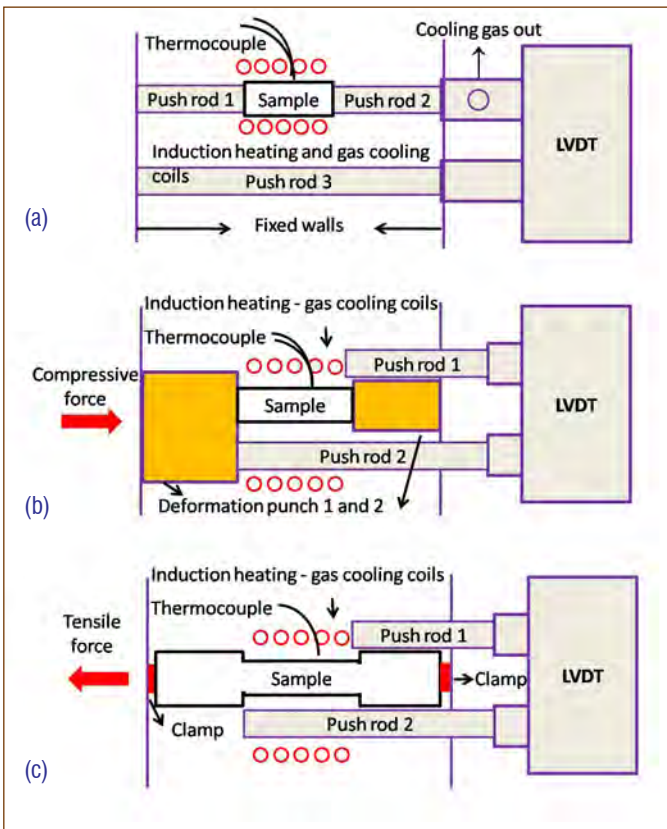


Figure 2: Schematic shows arrangement of push rod and samples in (a) Quenching (b) compression and (c) Tensile modes

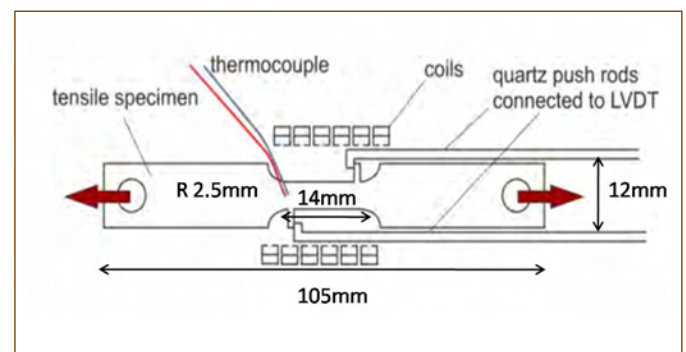


Figure 3: Schematic of tensile sample used in QDDL

Table 2: Chemical composition (in wt.%) of P9, P91 and BP91 steels used in this study

Material	Elements (in wt.%)									
	Fe	Cr	Mo	V	Nb	Ni	Mn	C	N	B
P9	Bal.	9.2	1.0	-	-	1.12	0.63	0.1	0.02	-
P91	Bal.	8.7	0.9	0.18	0.05	0.1	0.46	0.1	0.05	-
BP91	Bal.	9.2	1.0	0.21	0.07	0.01	0.5	0.1	0.011	0.006

paragraphs. Compositions of the materials used in these studies are given in Table 2.

CCT diagrams for P9 & P91 F/M steels:

CCT diagrams help in understanding phase transformation kinetics under non-isothermal conditions at different cooling rates and is a very useful tool during processing and welding of materials. CCT diagrams generated for P9 and P91 Ferritic-Martensitic (F/M) steels are shown as Figure 4(a) and (b) respectively. P9 and P91 steels were austenitized at 1050⁰C for 1h and 1000⁰C for 0.5h respectively and cooled at different cooling rates ranging from 0.05 to 20K/s. For both the steels the critical cooling rate for martensitic transformation is 0.1K/s (6K/min). Below the critical cooling rate, in P9, ferrite formed with starting and ending temperatures in the range of 820-824⁰C and 700-693⁰C respectively whereas in P91, ferrite formation temperatures were slightly lower with the starting and end temperatures obtained as 785-757 ⁰C and 690-560⁰C respectively. Ferrite formation subsequently affected the martensite transformation characteristics, which gets reflected in the Ms and Mf temperatures. For cooling rates <0.1K/s, Ms and Mf are in the range of 389-394⁰C and 350-354⁰C respectively for P9 and 280-

360⁰C and 320-280⁰C respectively for P91. For cooling rates faster than 0.1K/s, both Ms and Mf are independent of the cooling rates with their values obtained as (384⁰C, 332⁰C) and (357⁰C, 278⁰C) respectively for P9 and P91 steels respectively.

Isothermal transformation of γ -austenite to α -ferrite in P91:

P91 F/M steel was heated to 1000⁰C for 30min, then cooled to various temperatures ranging from 600⁰C to 800⁰C and held at these temperatures for 8h to study isothermal transformation of γ -austenite to α -ferrite. $\gamma \rightarrow \alpha$ transformation involves expansion as shown in Figure 5(a). Change in the length of the specimen was negligible during heat treatment at 600⁰C and 800⁰C indicating absence of phase transformation within the experimental time frame. At 650⁰C, transformation started after 3.5h and did not get completed until 8h whereas at 750⁰C transformation starting and completion could be clearly detected at 1.9h and 4.7h respectively. Fastest transformation kinetics were obtained after isothermal treatment at 700⁰C implying that this temperature marks the nose of the TTT diagram where both driving force and diffusion of substitutional elements are sufficient for faster kinetics. At higher temperatures i.e 750 and 800⁰C though diffusion kinetics is faster,

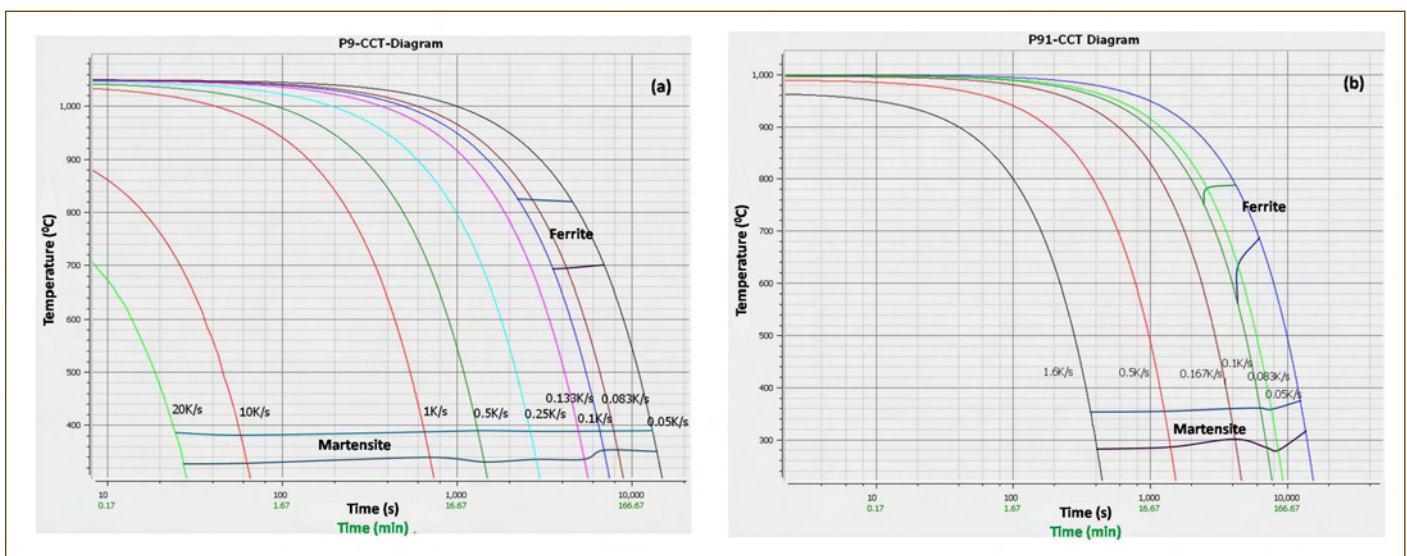


Figure 4: CCT diagram for (a) P9 and (b) P91 F/M steels

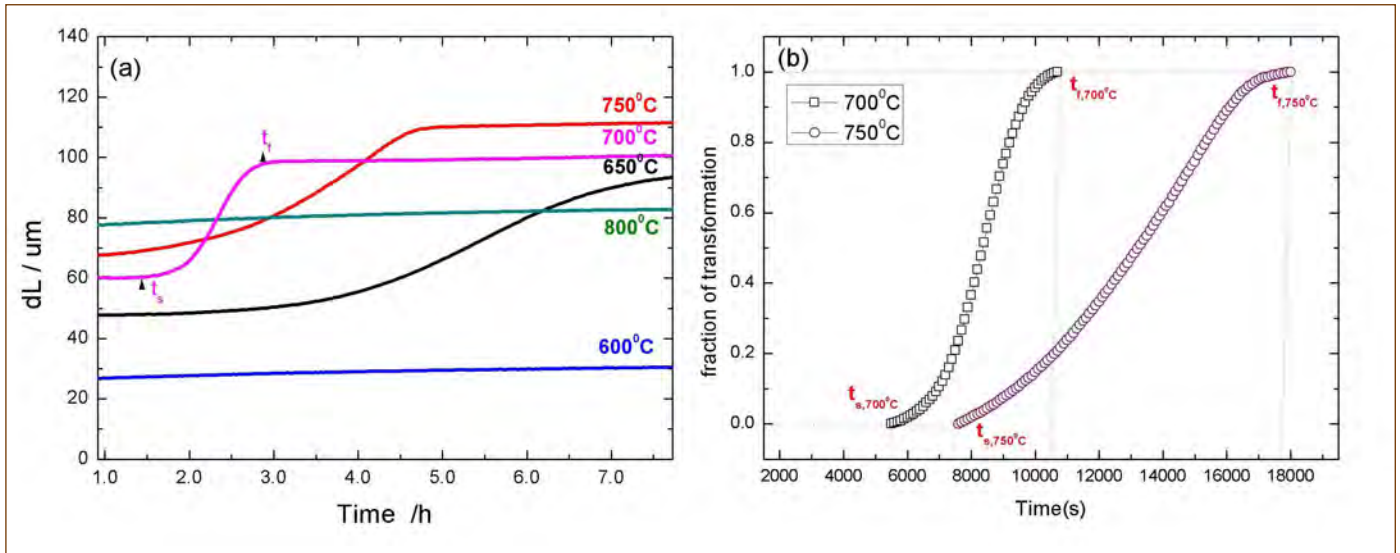


Figure 5:(a) Isothermal transformation behaviour of P91 (ts & tf represent starting and end time of transformation at 7000C (b) plot of fraction transformed vs time at 700 and 7500C

driving force is not sufficient whereas at low temperatures (600 and 650°C) despite high driving force slower diffusion results in incomplete transformation.

Apart from substitutional diffusion and driving force, another factor to be considered is precipitation of $M_{23}C_6$ and MX type carbides. During austenitization most of these precipitates may dissolve and re-precipitation is possible during holding at various temperatures. It is known that precipitation at γ/α boundary can affect the phase transformation kinetics. In the present study classic sigmoidal behaviour is observed for the phase transformation kinetics at

700°C but not for 750°C (Figure 5(b)). Interphase precipitation could be one of the reasons for the non-sigmoidal behaviour observed at 750°C.

Austenitization of P91 and BP91 during continuous heating:

Type IV cracking in HAZ of F/M steel is common mode of failure during creep which is however not observed in boron added P91 (BP91) steels. This may be a due to different mode of austenite transformation in BP91 steels under fast heating conditions prevailing during welding. To study these aspects, CHT diagrams were generated for P91 and BP91 steels during heating up to

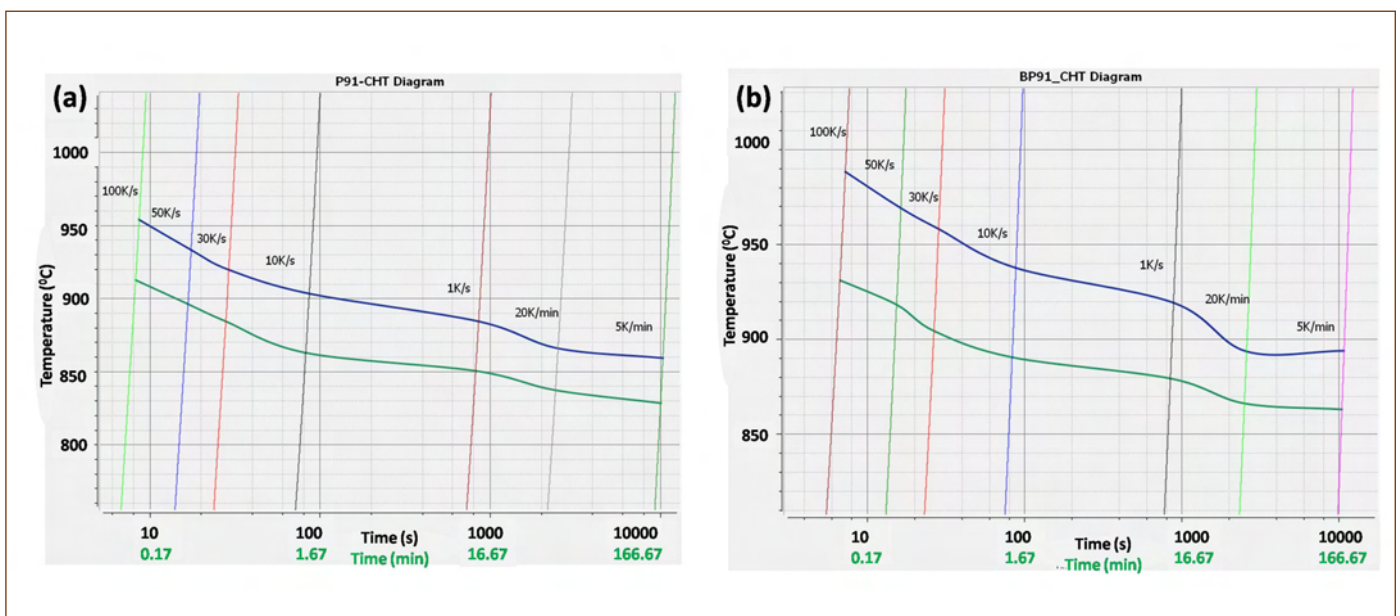


Figure 6: CHT diagrams for a) P91 and b) BP91 F/M steel

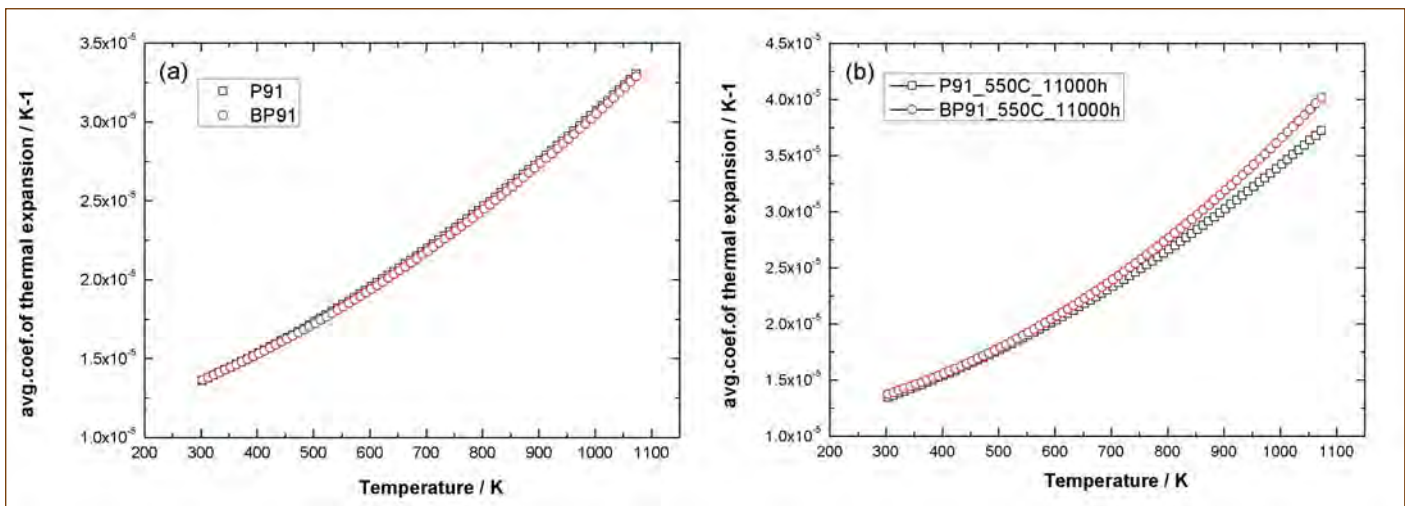


Figure 7: Temperature dependent variation of α_{avg} for (a) N&T and (b) aged P91 and BP91 F/M steels

1100°C at different heating rates (HR)

ranging from 5K/min to 100 K/s (Figure 6). As the heating rate increased from 5K/min to 100K/s, Ac1 and Ac3 are in the range of 830-910°C and 860-955°C for P91 and 860-930°C and 890-990°C for BP91. It is known that both Ac1 and Ac3 will increase with heating rate. In the present study it is observed that with increase in HR, difference (Δ) between Ac1 and Ac3 also increased for both the steels. Up to 20K/min, Δ is almost the same for both the steels. However at HR > 20 K/min, Δ had a higher value of 26°C in BP91 compared to ~11°C in P91 steels. This difference indicates a possible variation in the transformation mode of BP91 at higher HR. At low HRs, transformation proceeds by diffusional process i.e by nucleation and growth of austenite. This mode shows no difference between BP91 and P91. At higher HRs, diffusion less or shear transformation is likely to proceed which seems to be different for the two steels. Further investigations are in progress to understand such differences more clearly. Interestingly, mode of austenite transformation from ferrite did not affect martensite transformation. For both P91 and BP91, Ms and Mf temperatures are in the range of 355-365°C and 305-320°C respectively, irrespective of heating rates.

Effect of ageing on coefficient of thermal expansion:

BP91 shows better resistance than P91 during creep. Aim of the present study was to find variation in the average coefficient of

thermal expansion (α_{avg}) with aging of P91 and BP91 steels. Both steels were aged at 550°C for 11000h, then heated upto 800°C at a heating rate of 5K/min to identify changes in α_{avg} with temperature.

Measured temperature dependent variation in dilatational strain was used to calculate α_{avg} using the following equation

$$\alpha_{avg} = 1/l_{298} (dl/dT)$$

In the normalized and tempered (N&T) condition no discernible difference existed in α_{avg} between the two steels (Figure 7(a)) with the value varying in the range of 1.36 to 3.29x10⁻⁵ K⁻¹ in the temperature range of 30-800°C. Aged BP91 had slightly higher α_{avg} beyond 427°C. Observed change in thermal expansion could be linked to concurrent variation in microstructure. It is known that precipitation can lead to distorted interface with the matrix phase. Distorted interface is a result of different lattice parameters or different elastic properties of the phases involved. Coarsening of the precipitates is expected to reduce the distorted volume and increase thermal expansion. According to this explanation coarsening rate of M₂₃C₆ in BP91 must be higher - which is in contrast to the microstructural observations. Another possibility is that ageing can induce interphase boundary movement and formation of subgrains. Difference in the orientation of martensitic laths and subsequent formation of subgrain structure may be reason for higher α_{avg} of aged BP91 steel despite low coarsening rate of M₂₃C₆.

News and Events

4th AC & Refrigeration Service Program - ACRESERVE 2021

October 08, 2021



Shri V.Rathnakumar, Convener- ACRESERVE, Shri VijayaBhaskaran, RD South -2, ISHRAE HQ , Dr. K. Ananthasivan, Director, RpG, Shri Kesavan Nair, AD, TSG, ESG, Shri Biswanath Sen, Head, ACVSD and Shri V. Suresh Kumar, President ISHRAE Kalpakkam Chapter during inaugural function

Air-Conditioning & Ventilation System Division (AC&VSD), IGCAR in association with Indian Society of Heating Refrigerating & Air-conditioning Engineers (ISHRAE) - Kalpakkam Chapter organized the 4th AC & Refrigeration Service Program at Conference room, ESG Annex building, IGCAR on October 08, 2021. ACRESERVE is a training programme in Air conditioning and Refrigeration - Service conducted for technicians and contractor workers engaged in operation, Maintenance and service of HVAC equipments and systems. About 60 delegates (Technicians & Contract workers) from DAE units at Kalpakkam and ISHRAE Kalpakkam chapter members attended the training Programme in batches following safety protocols.

The conference started with the warm welcome address by Shri Biswanath Sen, Chairman ACRESERVE & Head, AC&VSD, ESG. Shri V. Suresh Kumar, President ISHARE Kalpakkam & Head, RFS, CFED addressed the gathering and briefed about ISHRAE and its activities. Shri K.P. Kesavan Nair, AD, TSG indicated about the necessity of such a training program. Shri V. Rathnakumar Convener, ACRESERVE and Head, ACMS, ACVSD highlighted about ACRESERVE. The chief guest of the inaugural function was Dr. K. Ananthasivan, Distinguished Scientist and Director, RpG, IGCAR. In his keynote address, Dr. K. Ananthasivan emphasized the importance of air quality in human life. He also enlightened on requirement of proper ventilation in buildings including radioactive facilities.

Shri Vijayabhaskaran, RD South-2, ISHRAE HQ delivered a useful talk on "Best Practices in Maintenance and Operation of HVAC system for energy efficiency". Other topics covered in the training programme include Basics of AC & Refrigeration, ISHRAE COVID -19 guidelines for offices and Residents, Electrical Safety for operation of HVAC, Introduction to Radioactive Ventilation – Operation & Maintenance of Systems, Good practice of Erection, testing & commissioning of Split & Window Air conditioners, Best way of Operation & Maintenance of Centrifugal Chillers and Basic understanding of Instrumentation. The talks were delivered by in house experts from ESG,RpG, and MCMFCG. Additionally, a Workshop demo on operation was organized on different types of compressors and Brazing Techniques.

During the valedictory function, Participation certificates were distributed to the delegates and the training programme facilitated good interactions among delegates and experts in the area of HVAC. Shri M.Ravi, President (Elect) ISHRAE Kalpakkam proposed the vote of thanks.

*Reported by
Shri Biswanath Sen, Head,AC-VSD-IGCAR*

News and Events

Dedication of 750 TR Capacity Centrifugal Chiller at Central Water Chilling Plant – II

October 13, 2021



Dr. B. Venkatraman, Distinguished Scientist & Director, IGCAR along with Senior Colleague dedicated during the first 750 TR capacity Centrifugal Chiller at CWCP - II to the centre

Central Water Chilling Plant-II [CWCP-II] is established by Air-Conditioning & Ventilation System Division [AC&VSD] to augment the central air-conditioning infrastructure of IGCAR. CWCP-II is designed to house four 750 TR capacity water cooled chiller and three 375 TR capacity air cooled chillers. The piping system is designed to take up an operating air-conditioning load of 3000 TR considering the future requirement. The new plant will cater to the air-conditioning demand of existing buildings - Training School and Training Centre, Material Science Laboratory (MSL), Material Development Laboratory (MDL), Condensed Matter Physical Laboratory (CMPL), Particle Irradiation Facility (PIF), Electronics and Instrumentation Laboratory (EIL) to name a few. The plant will also be useful in replacing the standalone packaged and unitary AC systems in various buildings which are at the end of their useful life. As phase I of the project, two 750 TR capacity centrifugal chillers are installed and commissioned with chilled water pumps, condenser cooling water pumps, cooling towers and associated piping network.

Dr. B. Venkatraman, Distinguished Scientist & Director, IGCAR dedicated the first 750 TR capacity Centrifugal Chiller at CWCP - II to the Centre in a ceremony organized by AC&VSD. Senior officials of the Centre, Dr. S. Raju, Director, MSG & MMG; Shri K. R. Sethuraman, CAO, IGCAR and Shri V. Sivakumar, IFA, IGCAR graced the occasion. Serving & retired colleagues from Engineering Services Group were also present in the memorable occasion. Shri Biswanath Sen, Head, AC&VSD has briefed regarding operational features and highlights of 750 TR centrifugal chiller and future plan of Central Water Chilling Plant-II. Shri K.P. Kesavan Nair, AD, TSG congratulated ACV, Civil and Electrical colleagues for completing the works within shortest possible time observing all the COVID protocols. Director, IGCAR has appreciated the efforts of AC&VSD in developing air-conditioning infrastructure to mitigate air conditioning problems.

As a customary, Dr. Venkatraman has recorded his invaluable remarks quoted as "A good initiative completed in time. Appreciate the entire ESG for this and request them to continue excellent and selfless services being rendered to the Scientific and Engineering cum Admin & Acct. community. Jai hind." on the equipment log book. Director, IGCAR has also planted a *Mimusops elengi* (Magilam) plant at CWCP-II premises to mark the remembrance of the event.

*Reported by
Shri Biswanath Sen, Head, AC-VSD-IGCAR*

News and Events

One Day Theme Meeting on SQUID Sensor and Its Applications

November 16, 2021



Some photographs of the event

A one day theme meeting on the applications of Superconducting Quantum Interference Device (SQUID) sensors for biomedical and geomagnetic research was conducted on November 16, 2021. With the welcome address by Dr. N. V. Chandra Shekar, Associate Director, MSG the meeting was inaugurated by Dr. S. Raju, Director, Materials Science Group. An introduction to the theme meeting was given by Mr. R. Baskaran, Head, SQUIDS and Applications Section. Dr. T. S. Radhakrishnan, Former Head, MSD, IGCAR gave the key note address. There were three technical sessions respectively dedicated to Biomagnetism, Time domain electromagnetic (TDEM) system and presentations by research scholars on recent developments in SQUID based applications. The first session on biomagnetism was chaired by Dr. M. Vineetha, Head-Pediatrics, DAE Hospital, Kalpakkam. Dr. Sanjib Sinha, Head, Department of Neurology, NIMHANS, Bengaluru presented a talk on the clinical applications of magnetoencephalography (MEG). Dr. Goutham K. Bhargava a senior resident of NIMHANS presented his work on the use of advanced machine learning algorithms applied to MEG signals. Dr. Santhosh Satheesh, Professor, Department of Cardiology, JIPMER, Pondicherry, emphasized the importance of early diagnosis of cardiovascular diseases and highlighted the role of MCG from a diagnostic perspective. Mr. S. Sengottuvel, SAS, MSG, IGCAR presented an overview of investigations conducted using the 37 channel MCG facility at Kalpakkam in collaboration with hospitals and medical institutions in the neighbourhood. The second session was on the TDEM applications of SQUID chaired by Dr. K. Gireesan. Dr. Ijee Mohanty presented her work on the geophysical prospecting done at Tumallapally, Kadappa district, Andhra Pradesh using the TDEM system. Ms. Lata Bisht, SAS, CMPD, MSG, presented her work on transient eddy current based non-destructive testing to measure the thickness of metal sheets and demonstrated the accuracy of the technique using simulation and actual measurements. Dr. R. Nagendran, gave an excellent account of a specific research problem probed using SQUID based TDEM, namely the negative decay transients, which is poorly understood in the literature. The last session was exclusively devoted to presentation by students and was chaired by Dr. H. Anitha, Professor, MIT, Manipal, Karnataka. Mr. Pathan Fayaz Khan presented his work on the development of a complete biofeedback system for conducting MEG and EEG experiments. The technical session was followed by a discussion with senior members of the Group. Dr. M. Jayashree, Medical Superintendent (MS), DAE Hospital, Kalpakkam chaired the session. Ideas on taking the program forward towards clinical use of SQUID based MCG were discussed.

*Reported by**Dr. N. V. Chandra Shekar Associate Director, MSG, IGCAR,*

News and Events

International Hybrid Conference on Recent Advances in Information Technology (READIT)

November 24-25, 2021



Smt. S. Rajeswari, Convener READIT, Shri S. Ragupathy, Distinguished Scientist, Director, EIG & RTDG, Dr. G. Ravikumar, Head, SIRD, BARC, Prof. J. P. Singh Joorel, Director, Infflibnet and Shri E. Soundararajan, Secretary READIT releasing the souvenir at the inaugural function READIT.



Director Dr. B. Venkatraman, felicitating Smt. Prabavathy Soundarajan, Head, LISS, SIRD.

The Scientific Information Resource Division of IGCAR in association with the Madras Library Association - Kalpakkam Chapter (MALA- KC) organized the 12th biennial Conference on Recent Advances in Information Technology (READIT) in hybrid mode during November 24-25, 2021 at the Sarabhai Auditorium, IGCAR, Kalpakkam, with the theme 'Innovative Technologies for Sustenance of Libraries'. For the first time since 1995, READIT was organized as an international event. International participants were from INIS group, IAEA Vienna, Institute of Physics UK, Springer Nature Singapore, along with research scholars from Sri Lanka and Nigeria to name a few.

About three hundred delegates from the academic and public Libraries, Publishers, Research scholars and Book exhibitors attended the conference in Hybrid mode. In the inaugural function, Smt. S. Rajeswari, Convener READIT & Head SIRD delivered the welcome address. The function was presided over by Shri. S. Ragupathy, Distinguished Scientist, Director, EIG & RTDG, IGCAR. Dr. G. Ravikumar, Outstanding Scientist & Head, SIRD, BARC delivered a special address. The Chief Guest of the inaugural event, Prof. J. P. Singh Joorel, Director, Infflibnet, Gujarat delivered the inaugural address. The Conference Souvenir was released by Prof. J. P. Singh Joorel. Shri E. Soundararajan, Organizing secretary READIT, proposed the vote of thanks. Dr. G. Ravikumar inaugurated the exhibition of Book stalls. The conference included 15 technical talks by domain experts in the field of Library and Information Science. A total of 15 presentations delivered by Students, Research Scholars and Librarians were considered for best presentation awards. Three best paper awards were announced to the paper presentations. Commercial presentations by Publishers were also arranged.

Dr. Nithyanandham and Smt S. Prabhavathy and Shri Ganesan from SIRD, IGCAR, were facilitated with Lifetime achievement award and significant contribution to Library awards by Dr. B. Venkatraman, Distinguished Scientist and Director IGCAR. Also, the contributions of Sri Premkumar, SIRD for representing India from DAE, who had received a Bronze medal in the international para badminton conducted in Uganda, was felicitated on READIT stage by Director, IGCAR, President MALA and President MALA-KC. A panel discussion was conducted on the theme "Future trends in scientific publishing and resource subscription models". An academic librarian, a scientist, a publisher, a vendor and a research librarian were part of the discussion. The conference facilitated good interactions among young researchers, students, professionals and well-known speakers in the area of future technologies for libraries. The conference was concluded with the valedictory function. Shri E. Soundararajan delivered the welcome address, Smt. S. Rajeswari presented the conference summary. The valedictory address was given by Shri Athmalingam, Associate Director, RESG, IGCAR. He also presented the best paper awards and honoured the sponsors of READIT 2021. Dr. V. S. Srinivasan proposed the vote of thanks. Conference was on Webex and YouTube simultaneously.

Reported by

Smt. S. Rajeswari, Convener READIT & Head SIRD

News and Events

International Medal by Shri E. Premkumar of DAE in Uganda Para-Badminton International 2021

November 25, 2021



Honourable Chief Minister Shri M. K. Stalin along with Minister V. Meyyanathan and Shri E. Premkumar



Dr. B. Venkatraman, Director, IGCAR, has congratulated the extraordinary fete

Shri E. Premkumar, SA/E, is the official photographer of IGCAR. He has a keen interest in nature photography and is a dedicated badminton player. He regularly participates in Nationals and International Badminton events like All India Central Civil Services, All India Inter-Institutional Badminton Tournaments, Para-Badminton international etc. After he met with multiple injuries in his right leg, he concentrated in the Para-Badminton category. He got classified as Standing Lower 4 in the 2nd Fazza – Dubai Para-Badminton International in March 2019. Subsequently, he got selected through state and national para-badminton committees to represent India in International Para-Badminton tournaments. Shri E. Premkumar represented India in the Uganda Para-Badminton International held at Kampala from 15th to 21st November 2021. Other participants include Olympian Pramod Bhagat (Paralympic Gold Medalist), Manoj Sarkar (Paralympics Bronze Medalist), and other elite players who regularly represent India in International tournaments. Twenty-seven countries have participated in the Uganda Para Badminton International with 135 players and 265 entries. Shri E. Premkumar participated in three events, Men's Singles, Men's Doubles, and Mixed Doubles. In Quarter-Finals (Men's Doubles), he won the match against youth Asia champion Nehal Gupta & Sharadchandra Joshi (17-21, 21-14, 21-14) in a 35 minutes match.



Shri E. Premkumar in Uganda Para-Badminton International 2021

Sri E. Premkumar, for the first time from DAE, has won an International Para-Badminton Bronze Medal in the Uganda Para-Badminton International at Kampala on November 2021. Tamilnadu Government felicitated the para-badminton players. Dr. B. Venkatraman, Distinguished Scientist, Director, IGCAR, has congratulated the extraordinary fete during the international conference READIT held on November 25, 2021. Dr. Ananthasivan, Director, RPG, has honored Sri Premkumar with a souvenir during their weekly IANCAS meeting. Many other sports councils like Thanjavur Badminton association, Para-Badminton association of Tamil Nadu, ACE badminton academy, NESCO etc have celebrated his fete.



Shri E. Premkumar was felicitated by NESCO, Kalpakkam

Through this article IGCAR, DAE appreciate the young gentleman and record their appreciation for the achievement and the many laurels he would bring to DAE and India.

Reported by

Smt. S. Rajeswari, Head SIRD

News and Events

Technology Transfer of “Autonomous Gamma Dose Logger”

December 07, 2021



Transfer of IGCAR's Autonomous Gamma Dose Logger technology to M/s Ideal Sensors, Chennai on December 07, 2021. (From L-R): Shri S. Athmalingam (Associate Director, RESG, SQRMG), Dr. N. Subramanian (Head, Incubation Centre-IGCAR), Shri A. K. Gowri Ponraj and Ms. R. Krithika (both from M/s Ideal Sensors).

Autonomous Gamma Dose Logger (AGDL) is a radiation monitor developed at SQRMG, IGCAR to measure environmental radiation in a wide range from 100 nGy/hr to 5 Gy/hr. The AGDL uses Geiger-Muller tubes to measure the environmental gamma dose rate. It transmits the data through wireless communication and backs up the data in a portable data logger. The radiation monitoring system is powered by solar power system with battery backup, and is installable at any site with a mechanical structure. This system can be used for both routine and emergency radiation field monitoring purposes in nuclear installations and as a general environmental radiation monitoring equipment in other places. IGCAR's AGDL has distinct features such as wireless (RF) communication, off-line local data logging, rapidly and remotely deployable even across rough terrains and seamless expansion of networking. Valuable inputs for Emergency Decision Support System can be provided by the AGDL. Currently ~28 numbers of in-house made AGDL systems are operating successfully at DAE Kalpakkam site and connected to the Decision Support System for real-time radiation field inputs.

The AGDL technology, developed to meet the Atma Nirbhar Bharat goals of our government, was transferred to M/s Ideal Sensors, Chennai on December 07, 2021. In a brief event arranged by Incubation Centre-IGCAR, the technology license documents were handed over by Shri S. Athmalingam, Associate Director (RSEG, SQRMG) to Ms. Krithika Rajagopalan and Shri A. K. Gowri Ponraj from M/s Ideal Sensors, Chennai. Dr. N. Subramanian, Head, Incubation Centre-IGCAR, Dr. C. V. Srinivas, Head, EAD, SQRMG, Dr. S. Chandrasekaran, Head, EnAS, EAD and other colleagues from SQRMG and IC-IGCAR attended the event. For more information on this technology and various other technologies developed at IGCAR, IC-IGCAR can be contacted at the email id: incubation@igcar.gov.in.

Reported by

Dr. N. Subramanian, Head, Incubation Centre-IGCAR,



Awards and Honours



Dr. Sandip Dhara, Materials Science Group: A Fellow of the Institute of Physics, England (October 2021).

Dr. John Philip, World's Top 2% Scientist in career ranking with a rank of 1,24,776

Dr. John Philip, World's Top 2% Scientist in (2021) ranking with a rank of 56,477

Dr. M. Vasudevan, World's Top 2% Scientist in career ranking with a rank of 2,24,331

Dr. M. Vasudevan, World's Top 2% Scientist in (2021) ranking with a rank of 1,16,119

Dr. Sandip Dhara, World's Top 2% Scientist in (2021) ranking with a rank of 2,30,595

Aritra Sarkar Selected as Member of "INYNAS" for the period 2022-2026 by Indian National Young Academy of Sciences

Aritra Sarkar awarded Alexander-von-Humboldt Research Fellowship by AvH Foundation, Germany to conduct research at the University of Siegen, Germany and Institute of Physics of Materials Czech Academy of Science, Brno

E. Premkumar, SIRD, IGCAR won the Bronze medal on Uganda Para-badminton International tournament 2021. In addition, outstanding contribution award in recognition of the dedicated efforts in the Biodiversity documentation was awarded by Madras Library Association Kalpakkam Chapter (MALA KC)



Best Paper/Poster Awards



Best Poster Award

Rangoli Hareesh, E. Vetrivendan, Ravikumar Sole and S. Ningshen

Steam Oxidation of CVD Synthesized Pyrolytic Graphite at Different Pyrolysis Temperature for High Temperature Application, CORCON - 2021, November 18 - 20, 2021 at NACE International Gateway India Section (Virtual mode)

Bio-diversity @ DAE Campus, Kalpakkam

Indian Golden Oriole



© SIRD, IGCAR

Indian Golden Oriole is medium sized bird and mostly seen in pair around the DAE kalpakkam complex. Both male and female are similar in size, but different in color. It has bright yellow head and body; a small black eye patch; wings and tails are black with yellow shades

Editorial Committee Members: Ms. S. Rajeswari, Dr. V. S. Srinivasan, Dr. John Philip, Dr. T. R. Ravindran, Dr. C. V. S. Brahmananda Rao, Shri A. Suriyanarayanan, Shri M. S. Bhagat, Shri G. Venkat Kishore, Dr. Girija Suresh, Shri M. Rajendra Kumar, Shri S. Kishore, Shri Biswanath Sen, Dr. N. Desigan, Shri Gaddam Pentaiah and Shri K. Varathan